A subset of UPR-induced transmembrane proteins are prematurely degraded during lipid perturbation

Benjamin S.H. Ng, Peter Jr. Shyu, Nurulain Ho, Ruijie Chaw, Seah Yi Ling, Guillaume Thibault

School of Biological Sciences, Nanyang Technological University, Singapore, 637551

Correspondence to:

Guillaume Thibault, Tel: +65 6592 1787; Fax: +65 6791 3856; email: thibault@ntu.edu.sg

Running title: Lipid perturbation destabilises a subset of transmembrane proteins

ABSTRACT

Background: Phospholipid homeostasis in biological membranes is essential to maintain functions of organelles such as the endoplasmic reticulum. Phospholipid perturbation has been associated to non-alcoholic fatty liver disease, obesity and other metabolic disorders. However, in most cases, the biological significance of lipid disequilibrium remains unclear. Previously, we reported that *Saccharomyces cerevisiae* adapts to lipid disequilibrium by upregulating several protein quality control pathways such as the endoplasmic reticulum-associated degradation (ERAD) pathway and the unfolded protein response (UPR).

Results: Surprisingly, we observed certain ER-resident transmembrane proteins (TPs), which form part of the UPR programme, to be destabilised under lipid perturbation (LP). Among these, Sbh1 was prematurely degraded by fatty acid remodelling and membrane stiffening of the ER. Moreover, the protein translocon subunit Sbh1 is targeted for degradation through its transmembrane domain in an unconventional Doa10-dependent manner.

Conclusion: Premature removal of key ER-resident TPs might be an underlying cause of chronic ER stress in metabolic disorders.

Keywords: Transmembrane protein degradation, Sbh1, phosphatidylcholine imbalance, chronic ER stress, unfolded protein response, ER protein quality control, ERAD, Doa10 complex, NAFLD, NASH.

BACKGROUND

Phospholipid homeostasis is crucial in the maintenance of various cellular processes and functions. They participate extensively in the formation of biological membranes, which serve to generate distinct intracellular environments into ordered compartments known as organelles for metabolic reactions, storage of biomolecules, signalling, as well as sequestration of metabolites. Existing as various and distinct species, phospholipids are regulated within relatively narrow limits and their composition in biological membranes among organelles differs significantly [1].

Perturbation of the two most abundant phospholipids, phosphatidylcholine (PC) and phosphatidylethanolamine (PE), can lead to various disease outcomes including non-alcoholic fatty liver disease (NAFLD) [2-5], type II diabetes (T2D) [6], as well as cardiac and muscular dystrophies [7]. Being highly abundant in biological membranes, the perturbation of PC and PE levels results in endoplasmic reticulum (ER) stress [8]. For instance, an elevated PC/PE ratio in obesity was found to contribute to the development of NAFLD [9, 10]. Perturbation in phospholipids was shown to cause the premature degradation of the sarco/endoplasmic reticulum Ca^{2+}-ATPase (SERCA) ion pump, disrupting calcium homeostasis and resulting in chronic ER stress [9]. This eventually led to hepatic steatosis and liver failure. In another study, mice fed with high fat diet exhibited an increase in gut microbiota enzymatic activity that have been shown to reduce choline [11, 12]. Choline is an essential dietary nutrient primarily metabolised in the liver and used for the synthesis of PC. Similarly, choline deficiency may play an active role in the development of insulin resistance. However, the development of chronic ER stress and metabolic diseases from lipid perturbation (LP) remains largely unknown.

In *Saccharomyces cerevisiae*, *de novo* synthesis of PC is catalysed by the enzymes Cho2 and Opi3, and similarly carried out by the homologue of Opi3, PEMT, in mammals (Fig. 1a). Cho2 first methylates PE to *N*-monomethyl phosphatidylethanolamine (MMPE), which is further methylated by Opi3 to PC through the intermediate *N*,*N*-dimethyl phosphatidylethanolamine (DMPE). Alternatively, PC is synthesised from choline, when available, through the Kennedy pathway. Both pathways are highly conserved from yeast to humans. It has been reported that *PEMT*$^{-/-}$ mice develop NAFLD within

three days of choline deficient diet [5]. Previously, we developed a LP yeast model to mimic NAFLD by deleting the gene *OPI3* [13].

The unfolded protein response (UPR) is a stress response pathway monitoring ER stress to restore cellular homeostasis [14]. Upon accumulation of misfolded proteins, the UPR is activated and alleviates stress by reversing severe dysfunctions through the upregulation of nearly 400 target genes in yeast [15]. Major targeted regulatory pathways includes cytosolic protein quality control (CytoQC), ER-associated degradation (ERAD), protein translocation, protein modification and phospholipid biosynthesis [15, 16]. By increasing ER protein folding capacity and enhanced clearance of misfolded proteins coupled with a general attenuation of protein translation [17], the UPR aims to achieve ER homeostasis.

Recently, it was demonstrated that the UPR is essential in alleviating ER stress in lipid dysregulated cells to maintain protein biogenesis, protein quality control and membrane integrity [13, 18-20]. LP, by the absence of *CHO2* or *OPI3*, exhibits synthetic lethality with the sole UPR signalling transducer in yeast, *IRE1*, as well as its downstream transcription factor *HAC1* [19, 20]. LP has been well characterised to induce ER stress [21-23], and the failure of the UPR to restore homeostasis is implicated in several human diseases [24-26]. This clearly establishes the critical role of the UPR in buffering the lethal effects of LP to ensure cell survival.

In this study, we observed certain ER-resident transmembrane proteins (TPs), part of the UPR programme, to be prematurely degraded under LP. First, we demonstrated that LP affects the ER membrane which results in the destabilisation of the TPs. Furthermore, we elucidated the mechanism of how one such TP, Sbh1, gets recognised for degradation through ERAD. Our findings reveal that under LP, Sbh1 transmembrane degron becomes accessible to the Doa10 complex leading to its premature degradation.

RESULTS

A subset of transmembrane proteins is destabilised during lipid perturbation

Global transcriptional and proteomic analyses from our previous work indicated a dramatically altered biochemical landscape in yeast cells under LP [13]. Among these, 66 proteins were identified to be transcriptionally upregulated, yet displayed a decrease in protein abundance (Table S1), including 11 ER-resident TPs. From these, we analysed the steady-state levels of ten TP candidates in cells under LP using the PC-deficient strain *opi3*Δ (Fig. 1a-b) [13]. Coy1, Cue1 and Erp5 exhibited similar protein steady-states in *opi3*Δ and WT, while Ctr1, Nsg2, Sbh1 and Scs7 had significantly lower steady-state levels. Surprising, Emc4, Prm5 and Yet3 showed higher steady-state protein levels. To exclude possible cellular functions affected from LP such as transport and secretion, we focused on ER-resident proteins by focusing on Cue1, Emc4, Nsg2, and Sbh1. Cue1 is an essential component of the ERAD pathway [27]. Emc4 is a member of the conserved ER transmembrane complex (EMC) and is required for efficient folding of proteins in the ER [21, 28]. The EMC is also proposed to facilitate the transfer of phosphatidylserine from the ER to mitochondria [29]. Nsg2 regulates the sterol-sensing protein Hmg2 [30]. Lastly, the β subunit of the Sec61 ER translocation complex, Sbh1, is highly conserved in eukaryotes and plays a role in the translocation of proteins into the ER [31-33]. Sbh1 is non-essential for translocation but leads to a defect in this process when deleted in conjunction with its paralogue, Sbh2 [34].

To assess the stability of TP candidates during LP, cycloheximide chase assay was performed in WT and *opi3*Δ strains. Half-lives of Emc4, Nsg2, and Sbh1 were found to be significantly reduced under lipid disequilibrium (Fig. 1c). No significant decrease in Cue1-HA protein level was detected in *opi3*Δ although the decrease was reproducible. One hour after attenuating protein translation, levels of Emc4, Nsg2, and Sbh1 were found to be 27%, 41%, and 58% lower in *opi3*Δ, respectively, compared to WT. This suggests that the UPR programme transcriptionally upregulates genes to restore ER homeostasis under LP, while a subset of TPs is recognised and targeted for degradation.

177 **A subset of ER-localised transmembrane proteins is destabilised by a decrease in**
178 **phosphatidylcholine**

179 To ensure that Cue1, Emc4, Nsg2, and Sbh1 remain as integral ER membrane proteins during lipid
180 perturbation, we verified their localisation at the ER (Fig. 2a) and their insertion into cellular
181 membranes (Fig. 2b) in *opi3*Δ cells. Together, these results suggest that integration into the ER
182 membrane is unaffected by PC depletion. To study the topology of these four proteins, we performed
183 proteinase K (PK) digestion from isolated microsomes (Fig. 2c). In WT cells, the C-termini HA tags of
184 Cue1-HA, Emc4-HA and Nsg2-HA are oriented towards the cytosol. Thus, the HA tag will be cleaved
185 off if the proper topology is preserved, while the detection of a HA-bearing peptide after PK digestion
186 indicates an inverted topology. The three proteins were found to be fully digested under LP and the
187 predicted smaller protein fragments of 23.7, 8.53, and 5.8 kDa were not detected for Cue1-HA, Emc4-
188 HA, and Nsg2-HA, respectively, in both WT and *opi3*Δ. Sbh1-HA is a tail-anchored protein where the
189 C-termini HA tag is found in the ER lumen. The predicted protein fragment of 10.5 kDa after PK
190 digestion was detected in both WT and *opi3*Δ strains, indicative of its correct membrane topology.
191 Typically, tail-anchored proteins are tagged at the N-termini as the C-termini interacts with the Get
192 complex for insertion into the ER membrane [35]. This result shows that, along with alkaline
193 carbonate extraction (Fig. 2b), adding a C-terminus HA tag to Sbh1 does not interfere with its
194 integration into the ER membrane. The four TPs were fully digested in the presence of the non-ionic
195 detergent Nonidet P-40 (NP40). Together, these findings suggest that the four TPs are prematurely
196 targeted for degradation once they are fully translated and integrated into the ER membrane.
197
198 To further confirm the four TPs are destabilised specifically from low PC levels, their degradation was
199 monitored in cells grown in the presence of choline to restore PC homeostasis (Fig. 1a) [13, 36].
200 Choline supplementation significantly stabilised Cue1-HA, Emc4-HA, Nsg2-HA, and Sbh1-HA in
201 *opi3*Δ to the levels of WT (Fig. 3a). Subsequently, we concentrated our effort on Sbh1 to better
202 understand how it is targeted for premature degradation during LP.
203
204 The UPR is strongly activated in response to LP [13, 21]. In *opi3*Δ, the UPR activation is constitutively
205 elevated and unresolved, thereby referred to as chronic ER stress [13, 37]. To ensure that Sbh1 is not
206 destabilised as a consequence of strong UPR activation, we introduced a constitutively active form of

207 the downstream effector, *HAC1*^{i}, into WT cells [16, 38]. As expected, *HAC1*^{i}-induced UPR activation
208 did not further destabilise Sbh1 in WT cells (Additional file 1: Fig. S1a). Noticeably, steady-state Sbh1
209 protein level is higher in UPR-activated WT cells as *SBH1* is upregulated from the UPR programme
210 [13, 15]. Additionally, yeast cells can mount an intact UPR in the absence of *SBH1* (Additional file 1:
211 Fig. S1b). Thus, this indicates that the UPR programme in *opi3*Δ is not sufficient to drive premature
212 Sbh1 degradation.
213
214 **Changes in ER membrane fluidity is sufficient to destabilise Sbh1**
215 To narrow down the specific effect of LP that might contribute to the premature degradation of Sbh1,
216 we analysed the fatty acid (FA) composition of whole cells and fractionated microsomes. Overall,
217 there was a general increase of cellular and microsomal (ER) saturated fatty acids (SFAs) and
218 decrease of monosaturated fatty acids (MUFAs) in *opi3*Δ when compared to WT (Fig. 3b). A
219 significant decrease of oleic acid (C18:1) was also observed in *opi3*Δ microsome fraction compared to
220 that of WT. In addition to FA remodelling, the intermediate for the synthesis of PC from PE, MMPE,
221 largely accumulates with the deletion of *OPI3* as we previously reported (Fig. 1a) [13]. A large MMPE
222 increase is expected to induce negative membrane curvature stress as has been reported for PE [39].
223 The remodelling of FA saturation state could be another adaptive response to alleviate membrane
224 curvature stress in *opi3*Δ [40, 41], as FA saturation states of biological membranes are highly linked
225 to membrane fluidity [42-44].
226
227 To better understand the impact of membrane remodelling on TPs behaviour, we monitored the
228 dynamics of the ER-resident membrane protein Sec63-sGFP by fluorescence recovery after
229 photobleaching (FRAP) [45]. A region of the cortical ER is photobleached and signal recovery
230 correlates with Sec63-sGFP mobility. The recovery of Sec63-sGFP fluorescence was significantly
231 slower in *opi3*Δ compared to WT suggesting rigidity of the ER membrane (Fig. 3c-e). This result is
232 consistent with previous reports on the effect of decreased PC/PE ratio in stiffening membranes [40,
233 46]. Taken together, it suggests that a decrease in membrane fluidity might prevent TPs to associate
234 to their interacting partners following translation and resulting in premature degradation.
235
236

Sbh1 binding to interacting partners is compromised under lipid imbalance

To further characterise the effect of LP on Sbh1 stability, we performed the split-ubiquitin based membrane yeast two hybrid (MYTH) screen in WT and *opi3*Δ cells to identify changes in Sbh1 membrane protein interactome [47, 48]. The reporter moiety was added at the N-terminus of Sbh1 (TF-C_{ub}-Sbh1) and did not compromise its ER localisation (Additional file 1: Fig. S2a). Strains expressing the Sbh1 bait were transformed with a yeast prey genomic plasmid library in which open reading frames are fused to sequences encoding the cognate reporter moiety [49]. A total of 49 and 14 putative Sbh1-interacting proteins were identified in WT and *opi3*Δ, respectively (Additional file 1: Fig. S2b). To eliminate false positive interactors, a bait dependency test was done using the single-pass transmembrane domain of the human T-cell surface glycoprotein CD4 tagged to C_{ub}-LexA-VP16 [49]. In WT, we identified 38 bona fide Sbh1 interactors including previously reported interactors Ost4, Sec61, Spc2, Ssb1, Sss1, and Yop1 (Fig. 4a) [50-53]. Sbh1 was also found to interact with membrane proteins involved in sterol biogenesis (Erg4, Erg24 and Nsg1) and fatty acid elongation (Elo2 and Tsc13). On the other hand, only 13 proteins were found to interact with Sbh1 in *opi3*Δ cells (Fig. 4b). No interaction of Sbh1 with Sec61 and Sss1 was detected in *opi3*Δ. This suggests that Sbh1 could be dissociated from the Sec61 complex under LP, and therefore causes its premature degradation. This is consistent with the finding that Sbh2, the paralogue of Sbh1, becomes destabilised and degraded rapidly when unbound to the Sec61-like complex Ssh1 [54]. Similarly, Sbh1 was found to interact with proteins of the ERAD pathway under LP (Fig. 4b). Sbh1 interactors include the membrane-embedded ubiquitin-protein ligase Doa10 which is part of the ERAD Doa10 complex [55, 56]. As the Doa10 complex is generally specific for substrates containing cytosolic lesions (ERAD-C) [57], it suggests that a polypeptide stretch of Sbh1 might become exposed on its cytosolic side under LP making it susceptible to ubiquitination. Subsequently, targeted substrates for degradation are polyubiquitylated in the cytosol by the addition of Lys-11-linked ubiquitin (Ubi4), a protein identified to interact with Sbh1 exclusively in *opi3*Δ cells. The AAA^+ ATPase protein Cdc48 was also found to interact with Sbh1 in *opi3*Δ cells (Fig. 4b). Ubiquitylated substrates are retro-translocated to the cytosol by the action of the Cdc48 complex and targeted to the proteasome for degradation [58, 59]. Another important player of the ERAD pathway, Png1, was found to exclusively interact with Sbh1 under LP. Png1 catalyses the deglycosylation of misfolded glycoproteins, and is a critical step for ERAD substrates modification to be fit for proteasomal degradation [60]. Together, the

MYTH screening results suggest that a change in membrane properties lead to the dissociation of Sbh1 from the Sec61 complex, resulting in its rapid degradation through the ERAD-C complex.

To ensure levels of the Sec61 complex subunits other from Sbh1 remain unchanged under lipid perturbation, we carried out cycloheximide chase assay to follow the stability of Sec61 and Sss1-Flag. Both Sec61 and Sss1 were found to be stable in *opi3*Δ as in WT in agreement with our previous proteomic data (Fig. 4c) [13]. To assess the interaction of Sbh1 with Sec61 complex on the ER membrane under LP, native co-immunoprecipitation (co-IP) was performed (Fig. 4d). In contradiction to the MYTH screen results, Sec61 was found to interact stably with Sbh1-HA in both WT and *opi3*Δ strains. The discrepancy could be due to the difference in membrane dynamics *in vivo* and *in vitro* from the MYTH and co-IP assay, respectively.

Sbh1 is destabilised from its transmembrane domain and degraded in a Doa10-dependent manner

To validate that Sbh1 is degraded in a Doa10-dependent manner, we carried out cycloheximide chase assay to monitor Sbh1 stability in different ERAD mutants. Sbh1 was found to be fully stabilised in *opi3*Δ*doa10*Δ but not in *opi3*Δ*hrd1*Δ and *opi3*Δ*usa1*Δ mutants (Fig. 5a). Hrd1 and Usa1 are both part of the Hrd1 complex which recognises lesions within the luminal domains of membrane and soluble proteins (ERAD-L) and those found within transmembrane region (ERAD-M) [61]. As some misfolded proteins in the ER are routed to the vacuole for degradation, we confirmed that Sbh1 degradation under LP is independent of the vacuolar pathway as shown by a similar degradation profile in *opi3*Δ*pep4*Δ. Conversely, Sbh1 degradation showed dependency on Cue1, a conserved element in both the Doa10 and Hrd1 complexes (Additional file 1: Fig. S3). Together with the MYTH data, it suggests that Sbh1 is exclusively targeted for degradation by the ERAD Doa10 complex.

To further elucidate how Sbh1 might be targeted for degradation by the Doa10 complex during LP, we mutated Sbh1 cytosolic lysine residues to alanine separately [Sbh1(K15A,K17A), Sbh1(K23A), Sbh1(K30A,K31A), and Sbh1(K41A)] and combined [Sbh1(6KA)]. The E3 ubiquitin-protein ligase Doa10 has been extensively reported to recognise ER proteins with cytosolic lesions resulting in the transfer of ubiquitin to lysine residues [62-69]. The degradation rates of Sbh1(K15A,K17A),

297 Sbh1(K23A), Sbh1(K30A,K31A), and Sbh1(K41A) expressed in *opi3*Δ cells were similar to unmutated
298 Sbh1 (Fig. 5b,c). Similarly, Sbh1(6KA) destabilisation was comparable to unmutated Sbh1 in *opi3*Δ
299 strain (Fig. 5d,e). Together, these findings suggest that Sbh1 is targeted for degradation by the Doa10
300 complex independently from the ubiquitination of its cytosolic domain. Yeast paralogue of Sbh1,
301 Sbh2, is degraded by Doa10 through an intramembrane degron [54]. Thus, we examined the
302 degradation of Sbh1 containing the transmembrane domain of Sbh2 in *opi3*Δ strain (Fig. 5f).
303 Replacing the transmembrane domain of Sbh1 was sufficient to stabilise it during LP suggesting the
304 degron recognised by Doa10 is within the lipid-embedded Sbh1 α-helix [54]. To further validate this
305 finding, we used a stable Sbh2 mutant wherein the two non-conserved amino acids of the
306 transmembrane domain of Sbh2 have been mutated from serine to proline and alanine at positions 61
307 and 68, respectively [Sbh2(S61P,S68A)]. These two point mutations drive Sbh2 native interaction
308 from the Ssh1 translocon to the Sec61 translocon. As previously reported, Sbh2(S61P,S68A) was
309 stable in WT cells (Fig. 5f). Unexpectedly, Sbh2(S61P,S68A) was similarly stable in *opi3*Δ cells,
310 suggesting the Sec61 translocon maintains its ability to interact with the non-essential β subunit.
311 Together these findings suggest that the Doa10 complex recognises the Sbh1 transmembrane
312 degron that becomes accessible during LP perhaps due to the change in the ER membrane
313 composition.
314
315
316 **DISCUSISON**
317 The strong association between obesity and non-alcoholic fatty liver disease (NAFLD) in human
318 populations is evident of the importance of lipid regulation in determining the emergence of fatty liver
319 pathogenesis: NAFLD is now the most common cause of chronic liver enzyme elevation and
320 cryptogenic cirrhosis, as a result of increased obesity [70, 71]. Total PC is consistently decreased in
321 NAFLD and non-alcoholic steatohepatitis (NASH) liver samples from human patients and mouse
322 models [8, 72, 73], and it correlates with a decrease of the enzyme required for *de novo* synthesis of
323 PC in the liver, PEMT [9, 73]. Concurrently, chronic ER stress and the activation of the UPR are both
324 associated with NAFLD pathologies [9, 74, 75]. Despite these connections, little is known on the effect
325 of phospholipid perturbation on pathways of the ER. Thus, we sought to better understand how the

ER fails to reach homeostasis under chronic PC depletion and how the protein quality control machinery is implicated using our previously reported yeast model system [13].

The proteostasis network undergoes extensive remodelling upon PC depletion in yeast [13]. Although a large subset of proteins is increased in these stressed cells, we noticed that key proteins are rapidly degraded and are indeed sensitive to phospholipid variations. Out of the 66 proteins which displayed decreased protein abundance despite being genetically upregulated, 40% are transmembrane proteins (TPs). As 30% of the proteome is predicted to be integral or peripheral membrane proteins [52], it suggests that TPs are more sensitive to LP compared to other types of proteins. Among the identified TPs, a large proportion are ER-resident proteins suggesting this organelle is more vulnerable to the effects of LP, and that this in turn affects TP integrity in the ER. The virtual absence of sterol at the ER, a key regulator of membrane fluidity, might contribute to its susceptibility to change in the biophysical properties of the membrane through lipid variation {Zinser, 1993 #871;Weete et al., 2010;Subczynski, 2017 #943}.

We sought to investigate changes in membrane properties under LP that caused the destabilisation of a subset of TPs. PC is cylindrically shaped with a cross-sectional area for the head-group similar to its constituent acyl chain tails, generating minimal curvature and forming flat lamellar phase phospholipid bilayers [76]. PE is classified as cone-shaped lipid forming non-lamellar membrane structure as it generates negative membrane curvature [39]. The phospholipid intermediate MMPE becomes highly abundant under the ablation of *OPI3*, and being mono-methylated, it has physical properties more similar to PE (Fig. 1a). The increase in membrane curvature from the replacement of PC to MMPE may induce cells to decrease their FA chain lengths in accordance to the seminal Helfrich theory of membrane bending elasticity (Fig. 3b) [41]. A more pronounced remodelling of the FA chain length in the ER over whole cell suggests either the ER is more susceptible to LP due to the minimal presence of ergosterol at the ER [77] or cells respond more aggressively to the ER membrane bilayer disruption to alleviate ER stress. Accordingly, a rise in membrane lipid packing from elevated saturated fatty acids will reduce the propensity to form curvatures.

355 However, the remodelling of the ER to alleviate negative membrane curvature stress, induced from
356 high PE and MMPE levels, can impose further challenges to cells. An elevation in saturated fatty acid
357 chains decreases ER membrane fluidity (Fig. 3b) [78] which might be partially due to the absence of
358 the rich unsaturated fatty acid provider, PC [79, 80]. Additionally, the replacement of PC with MMPE
359 contributes to the stiffening of the membrane [46]. Thus, these changes combined with the relatively
360 low abundance of ergosterol at the ER membrane bilayer make this organelle particularly susceptible
361 to PC level variations. Indeed, this change in the ER membrane led to the premature degradation of
362 Sbh1 by the Doa10 complex through a degron within the transmembrane domain of Sbh1. The loss of
363 Sbh1 interacting partners, during LP, might contribute to its degradation as reported for its yeast
364 paralogue Sbh2 [54]. Dissociation of Sbh2 from the Ssh1 complex (yeast Sec61 paralogue) was
365 proposed to sufficiently drive its Doa10-mediated degradation. Interestingly, none of the Sbh1
366 cytosolic lysine residues are required for its degradation through the Doa10 complex suggesting Sbh1
367 might by atypically ubiquitylated as has been reported for the Doa10 substrate Asi2 [81].
368
369 Alteration of lipid raft composition at the plasma membrane can lead to loss of protein function and
370 rapid degradation [79, 82, 83]. The rigidity of the ER membrane, from depleting PC, may interfere with
371 Sbh1 conformational changes necessary for its interaction with the Sec61 complex and thus result in
372 its degradation [84]. Alternatively, the stiffening of the lipid membrane may reduce Sbh1 diffusion
373 through the lipid bilayer leading to sustained interaction with the Doa10 complex (Fig. 4 and 6) [54,
374 85]. Thus, a decrease in PC clearly targets Sbh1 for degradation from a change in the biophysical
375 property of the membrane. It remains to be determined if the LP-induced degradation mechanism of
376 Sbh1 applies to the other destabilized TPs that have been identified (Fig. 1b). Additionally, the
377 absence of PC with its large head-group and the abnormally high presence of PE and MMPE with
378 smaller head-groups at the lipid membrane-cytosol interface should result in Doa10 accessibility of
379 the Sbh1 α-helix degron [54].
380
381 The coordinated upregulation of the proteostasis network by the UPR serves as an important stress
382 recovery mechanism that helps cells cope with the otherwise lethal effects of LP [13]. Despite this
383 robust stress response under LP, the UPR programme fails to increase the expression level of a
384 subset of TPs. The premature degradation of these TPs can prevent an effective proteostatic

response especially under prolonged LP (Fig. 6). ER stress induced from a temporary lipid perturbation will result in the upregulation of UPR target genes and consequently ER homeostasis. However, in the context of fatty liver, prolonged LP might prevent cells from reaching ER homeostasis by the premature degradation of key UPR target TPs. Therefore, this will lead to chronic ER stress which might contribute to the progression of NAFLD. In addition, the prolonged upregulation of lipogenic transcription factors from the UPR programme may also contribute to liver progression into hepatosteatosis [86].

In contrast, disrupting phospholipid homeostasis may be exploited to target pathogens. An increase in phospholipid synthesis is essential for replication of the parasite *Plasmodium falciparum* during the erythrocytic stage [87]. Phospholipid content of parasite-infected erythrocytes dramatically increases during maturation with 85% of newly synthesised phospholipids being PC and PE for growth and cell division [88]. Hence, the inhibition of phospholipid synthesis might be an effective strategy for antimalarial drugs [87, 89]. In addition, *P. falciparum* resistance to artemisinin-based combination therapies (ACTs) is associated to ER stress where the UPR mitigates artemisinin-induced protein damage [90]. Thus, targeting phospholipid biosynthesis in combination with artemisinin might be an efficient strategy to overcome resistance by preventing effective UPR activation in *P. falciparum*. [91]. Similarly, it may be applied to therapeutic strategies against diseases such as cancer where UPR activation is a potent driver of cell division [24, 92].

CONCLUSIONS

Here, we report that a subset of transmembrane proteins, part of the UPR programme, are prematurely degraded under LP. ER-resident proteins Cue1, Emc4, Nsg2, and Sbh1 topology and integration into the ER are not affected by LP while they are prematurely degraded. By further investigating the β subunit of Sec61 ER translocation complex, Sbh1, we proposed that it is prematurely degraded by the Doa10 complex through the recognition of a specific transmembrane degron. The proper association of Sbh1 with its interacting partners as well as the maintenance of membrane lipid PC level should be sufficient to prevent the Sbh1 degron from being recognised by the Doa10 complex during lipid equilibrium. However, the drastic decrease of PC associated with fatty

liver promotes the dissociation of Sbh1 from its interacting partners as well as the exposure of Sbh1 proline 54 leading to its premature degradation in a Doa10-dependent manner. Thus, the premature degradation of a subset of ER-resident TPs during prolonged lipid perturbation might contribute to chronic ER stress associated with NAFLD and NASH.

METHODS

Statistics

Error bars indicate standard error of the mean (SEM), calculated from at least three biological replicates, unless otherwise indicated. *P* values were calculated using two-tailed Student's t test, unless otherwise indicated, and reported as *P*=value in figures.

Strains and antibodies

Saccharomyces cerevisiae strains used in this study are listed in Additional file 1: Table S2. Strains were generated using standard cloning protocols. Anti-Kar2 polyclonal rabbit antibody and anti-Sec61 polyclonal rabbit antibody were gifts from Davis Ng (Temasek Life Sciences Laboratories, Singapore). Anti-HA mouse monoclonal antibody HA.11 (Covance, Princeton, NJ), anti-Pgk1 mouse monoclonal antibody (Invitrogen), anti-GFP mouse monoclonal antibody (Sigma-Aldrich, St. Louis, MO) anti-tubulin mouse monoclonal antibody 12G10 (DHSB) and anti-LexA polyclonal rabbit antibody (Abcam, Cambridge, United Kingdom) were commercially purchased. Secondary antibodies goat anti-mouse IgG-DyLight 488 (Thermo Fisher, Waltham, MA), goat anti-rabbit IgG-DyLight 550 (Thermo Fisher, Waltham, MA), goat anti-mouse IgG-HRP (Santa Cruz Biotechnology, Dallas, TX), goat anti-rabbit IgG-HRP (Santa Cruz Biotechnology, Dallas, TX), goat anti-mouse IgG-IRDye 800 (LI-COR Biosciences) and goat anti-rabbit IgG-IRDye 680 (LI-COR Biosciences, Lincoln, NE) were commercially purchased.

Plasmids used in this study

Plasmids and primers used in this study are listed in Additional file 1: Table S3 and S4, respectively. Plasmids were constructed using standard cloning protocols. All coding sequences of constructs used in this study were sequenced in their entirety. The plasmid pJC835 containing *HAC1*^{i} gene in pRS316

445 was previously described [14]. The plasmids pGT0179, pGT0181, pGT0183, and pGT0185, were
446 generated by amplifying the promoter and open reading frame of *NSG2*, *CUE1*, *SBH1*, and *EMC4*
447 with primer pairs BN033-034, BN029-030, BN035-036, and BN031-032, respectively, from the
448 template WT genomic DNA (gDNA). PCR products of *NSG2, SBH1,* and *EMC4* were digested with
449 the restriction enzymes *NotI* and *NcoI* before being ligated into the corresponding restriction sites in
450 pRS315. *CUE1* PCR product was digested with the restriction enzymes *NcoI* and *PstI* before being
451 ligated into the corresponding restriction sites in pRS315. The plasmid pGT0288 was generated by
452 amplifying the open reading frame of Sbh1 with primer BN027 and BN028 from WT gDNA and
453 digested with the restriction enzyme *SfiI* before being ligated into the corresponding restriction sites in
454 pBT3N. The plasmid pGT0350 was generated by Gibson assembly to join the promoter and open
455 reading frame of *SSS1* with primers BN013 and BN014 from WT gDNA with a 3X FLAG tag amplified
456 with primers BN015 and BN016 from pGT0284 into pRS313. Plasmids pGT0352, pGT0445,
457 pGT0446, and pGT0447 were generated by performing site-directed mutagenesis on pGT0183 with
458 primer pairs BN037-BN038, PS153-PS154, PS141-142, and PS143-144, respectively, as previously
459 described [93]. The plasmid pGT0459 was generated by sequential site-directed mutagenesis from
460 pGT0352 using primer pairs PS143-PS144, PS141-PS142, and PS139-140 as previously described
461 [93].
462
463 **Cycloheximide chase assay**
464 Cycloheximide chase assay was carried out as previously described [94]. Typically, 6 OD_{600} units of
465 early log phase cells were grown in synthetic media. Protein synthesis was inhibited by adding 200
466 µg/ml cycloheximide. Samples were taken at designated time points. Cell lysates from these samples
467 were resolved by SDS-PAGE and transferred onto a nitrocellulose membrane. Immunoblotting was
468 performed with appropriate primary antibodies and horseradish peroxidase-conjugated secondary
469 antibodies or IRDye-conjugated secondary antibodies. Proteins were visualised using the ECL system
470 (C-DiGit Chemiluminescent Western Blot Scanner) or the NIR fluorescence system (Odyssey CLx
471 Imaging System). Values for each time point were normalised using anti-Pgk1 or anti-Tub1 as loading
472 controls. Quantification was performed using an Odyssey infrared imaging program (LI-COR
473 Biosciences, Lincoln, NE).
474

475 **Indirect immunofluorescence**

476 Indirect immunofluorescence was carried out as previously described [95]. Typically, cells were grown
477 to early log phase at 30°C in selective synthetic complete media, fixed in 3.7% formaldehyde and
478 permeabilised. After blocking with 3% BSA, staining was performed using anti-HA (1:200), anti-LexA
479 (1:500), anti-GFP (1:200) or anti-Kar2p primary antibody (1:1,000) followed by Alexa Fluor 488 goat
480 anti-mouse secondary antibody (1:1,000) and goat anti-rabbit IgG-DyLight 550 (Thermo Fisher,
481 Waltham, MA). Samples were visualised using a Zeiss LSM 710 microscope with a 100x 1.4 NA oil
482 Plan-Apochromat objective (Carl Zeiss MicroImaging).

483

484 **Alkaline carbonate extraction**

485 Alkaline carbonate extraction was carried out as previously described [96]. Five OD_{600} units of early
486 log phase cells were resuspended in 1.2 ml of 10 mM sodium phosphate pH 7.0, 1mM PMSF and
487 protease inhibitor cocktail (PIC). An equal volume of 0.2 M sodium carbonate (pH 11.0) was added to
488 cell lysates incubated 30 min at 4°C and spun down at 100,000 x *g* for 30 min, 4°C. The pellet
489 (membrane fraction) was solubilised in 3% SDS, 100 mM Tris, pH 7.4, 3 mM DTT and incubated at
490 100°C for 10 min. Proteins from total cell lysate and supernatant fractions (collected from centrifuged
491 lysate) were precipitated with 10% trichloroacetic acid (TCA) and spun down 30 min at 18,400 x *g*,
492 4°C. Proteins were resuspended in TCA resuspension buffer (100 mM Tris-HCL pH 11.0, 3% SDS).

493

494 **Proteinase K digestion assay**

495 Fifty OD_{600} units of early log phase cells were pelleted and resuspended in 1 ml Tris Buffer (50 mM
496 Tris pH 7.4, 50 mM NaCl, 10% glycerol, 1mM PMSF and PIC). The clarified cell lysate was spun
497 down at 100,000 x *g* for 1 h at 4 °C. The pellet was resuspended and washed with 0.5 ml Tris Buffer
498 without PMSF and PIC. Around ~ 5 OD_{600} equivalent of microsomes were incubated with 1 mg/ml
499 Proteinase K (Promega, Fitchburg, WI) and 1% Nonidet P40 substitute (Sigma-Aldrich, St. Louis, MO)
500 when indicated and incubated at 37°C for 30 min. To quench the reaction, 5 mM PMSF was added
501 followed by TCA precipitation. Samples were resolved by SDS-PAGE and transferred onto a
502 nitrocellulose membrane. Immunodetection was performed with appropriate primary antibodies and
503 IRDye-conjugated secondary antibodies. Immunoreactive species were visualised using the NIR
504 fluorescence system (Odyssey CLx Imaging System).

505

506 **Lipid extraction and fatty acid analysis**

507 For whole cells, 10 OD_{600} of early log phase cells were pelleted, washed and resuspended with ice-
508 cold water and lyophilised using Virtis Freeze Dryer under vacuum. For lipid extraction for
509 microsomes, 50 OD_{600} of early log phase cells were pelleted, washed with phosphate-buffered saline
510 (PBS) and resuspended in 1 ml of Tris Buffer (50 mM Tris-HCL, 150 mM NaCl, 5 mM EDTA pH 8.0,
511 167 µM PMSF and PIC). The clarified lysate was spun down at 100,000 x *g* for 1 h at 4°C. The pellet
512 was resuspended in 100 µl ddH_2O and sonicated for 30 min. Lipid content was normalised to protein
513 content using bicinchoninic acid (BCA) protein assay (Sigma-Aldrich, St. Louis, MO). Normalised
514 microsome contents were resuspended with ice-cold ddH_2O and lyophilised using Virtis Freeze Dryer
515 under vacuum. Lyophilised samples were subjected to 300 µl 1.25 M HCl-MeOH (Sigma-Aldrich, St.
516 Louis, MO) and incubated at 80°C for 1 h to hydrolyse and esterify FAs into FA methyl esters (FAME).
517 FAMEs were extracted three times with 1 ml of hexane and separated on a gas chromatography with
518 flame ionization detector (GC-FID; GC-2014; Shimadzu, Kyoto, Japan) equipped with an Ulbon HR-
519 SS-10 capillary column (nitrile silicone, 25 m x 0.25 mm; Shinwa Chemical Industries, Kyoto, Japan).
520 The temperature was held 3 min at 160°C and increase to 180°C with 1.5°C/min increments and to
521 220°C with 4°C/min increments.

522

523 **Fluorescence recovery after photobleaching**

524 Fluorescence recovery after photobleaching (FRAP) was carried out as previously described [45].
525 Typically, early log phase cells expressing Sec63-sGFP were fixed on coverslips in Attofluor cell
526 chambers (Thermo Fisher, Waltham, MA) with concanavalin A before rinsing thrice with ddH_2O. Cells
527 were imaged for 5 s followed by photobleaching a region of interest of 82 x 82 pixels at 100% intensity
528 488 nm laser under 5 × magnification. Subsequently, images were taken at 1.57 s intervals for a total
529 of 160 sec. Images were acquired using a Zeiss LSM 710 microscope with a 100x 1.4 NA oil Plan-
530 Apochromat objective (Carl Zeiss MicroImaging) with argon laser line 488 nm of optical slices 4.2 µm.
531 ZEN black edition was used for image acquisition and analysis. Magnification, laser power, and
532 detector gains were identical across samples. For data analysis, the fluorescence intensities of three
533 regions of interest were measured for the duration of the experiment: the region of interest (ROI), a
534 region outside of the cell to measure the overall background fluorescence (BG), and a non-

photobleached region within the cell was monitored to measure the overall photobleaching and fluorescence variation (REF). Normalised fluorescence intensity [F(t)$_{norm}$] was calculated for each time point using Eq. 1 [97]. F(i) denotes the initial fluorescence intensities.

$$F(t)_{norm} = \frac{F(t)_{ROI} - F_{BG}}{F(t)_{REF} - F_{BG}} \times \frac{F(i)_{REF} - F_{BG}}{F(i)_{ROI} - F_{BG}} \quad (1)$$

Fluorescent recovery was analysed by calculating half maximal fluorescence intensity ($t_{½}$) using Eq. 2 [98]. F_0 denotes the normalised initial fluorescence intensity, F_∞ the normalised maximum fluorescence intensity and F(t) the normalised fluorescent intensity at each time point.

$$F(t) = \frac{F_0 + F_\infty \frac{t}{t_{1/2}}}{1 + \frac{t}{t_{1/2}}} \quad (2)$$

The $t_{½}$ values were plotted using GraphPad Prism 5.0.

Membrane yeast two-hybrid system assay

Membrane yeast two-hybrid (MYTH) assay was carried out as previously described [47]. Yeast two-hybrid screen uses the split ubiquitin two hybrid (N-terminus, N_{ub} and C-terminus, C_{ub}). Briefly, MYTH bait was generated by integrating C_{ub}-LexA-VP16 tag at the N-terminus of Sbh1 under the control of the promoter *CYC1* and transformed into the NMY51 yeast strain. Sbh1 tagged protein localization was verified by indirect immunofluorescence using anti-LexA antibodies against the tag described above. Seven micrograms of N_{ub}G-X cDNA prey library (Dualsystems) was transformed in 35 OD_{600} units of *SBH1* reporter cells. Interactors were isolated on selective complete (SC) media lacking tryptophan, leucine, adenine and histidine complemented with 80 µg/mL X-Gal and 5 mM 3-Amino-1,2,4-triazole (3-AT) and grown for two days at 30°C. The histidine inhibitor 3-AT was used to reduce false positive colonies. Only colonies which display robust growth on selective media and a blue colour were selected for further analysis. The prey cDNA plasmids were isolated and sequenced. The list of interactors was verified via the bait dependency test, wherein all identified interactors are retransformed back into the original bait strain, together with a negative control using the single-pass transmembrane domain of human T-cell surface glycoprotein CD4 tagged to C_{ub}-LexA-VP16 MYTH [49]. Interactors that activate the reporter system in yeast carrying the negative control bait were

562 removed from the list of interactors. Yeast that harbour the prey and the bait-of-interest and did not
563 grow were likewise removed from the list of interactors.
564
565 **Co-immunoprecipitation**
566 Native lysis protocol was carried out as previously described [99]. Briefly, 40 OD_{600} units of
567 exponentially growing early log phase cells were harvested and resuspended in 1 ml native lysis
568 buffer (50 mM Tris, pH 7.5, 150 mM NaCl, 5 mM EDTA, 1 mM PIC and 1 mM PMSF). Microsomes
569 were spun down from the clear lysates at 200,000 X *g* for 30 min, 4ºC. The pellet was solubilised in
570 native lysis buffer with 1% digitonin (Calbiochem) overnight at 4ºC. The resulting lysate was cleared
571 by centrifugation at 16,000 X *g* for 10 min, 4ºC prior to immunoprecipitation. Solubilised microsomes
572 were incubated with Protein G beads and anti-HA antibodies overnight at 4ºC. Beads were washed
573 thrice lysis buffer containing 0.5% digitonin and twice with TBS. Proteins were separated using SDS-
574 PAGE and visualised by immunoblotting as described above.
575
576 **β-galactosidase reporter assay**
577 The β-galactosidase reporter assay was carried out as previously described [16]. Typically, four OD_{600}
578 units of early log phase cells were collected and resuspended in 75 µl LacZ buffer (125 mM sodium
579 phosphate, pH 7, 10 mM KCl, 1 mM $MgSO_4$, 50 mM β-mercaptoethanol). As positive control to induce
580 the UPR, tunicamycin was added at a concentration of 2.5 µg/ml to growing WT cells 1h prior to
581 harvest. An aliquot of 25 µl cell resuspension was transferred into 975 µl ddH_2O and the absorbance
582 was measured at 600 nm. To the remaining resuspension, 50 µl chloroform and 20 µl 0.1% SDS were
583 added and vortexed vigorously for 20 sec. The reaction was started with the addition of 1.4 mg/ml
584 ONPG (2-nitrophenyl -D-galactopyranoside; Sigma) in LacZ buffer. Then, the reaction was quenched
585 with 500 µl of 1 M Na_2CO_3 when sufficient yellow colour had developed without exceeding a ten-
586 minute reaction. The absorbance was measured at 420 and 550 nm. The β-galactosidase activity was
587 calculated using Eq. (3).

588 $$\text{Miller units} = 1000 \times (OD_{420} - 1.75 \times OD_{550}) / (t \times (VA/VR) \times OD_{600}) \quad (3)$$

589 The values were then normalised to the activity of WT.
590
591

LIST OF ABBREVIATIONS

co-IP, co-immunoprecipitation; CytoQC, cytosolic protein quality control; DMPE, N-dimethyl phosphatidylethanolamine; ER, endoplasmic reticulum, ERAD, endoplasmic reticulum-associated degradation; FA, fatty acid; LP, lipid perturbation; MMPE, N-monomethyl phosphatidylethanolamine; MYTH, membrane yeast two hybrid; NAFLD, non-alcoholic fatty liver disease; NASH, non-alcoholic steatohepatitis; PC, phosphatidylcholine; PE, phosphatidylethanolamine; SERCA, sarco/endoplasmic reticulum Ca2+-ATPase; T2D, type II diabetes; TP, transmembrane protein; UPR, unfolded protein response.

DECLARATIONS

Ethics approval and consent to participate

Not applicable

Consent for publication

Not applicable

Availability of data and material

All data generated and/or analysed from this study are included in this manuscript and its additional information files

Competing interests

The authors declare that they have no competing interests.

Funding

This work was supported by the Nanyang Assistant Professorship program from Nanyang Technological University and the Nanyang Technological University Research Scholarship to B. S.H. N. and P.J.S. (predoctoral fellowship).

622 **Authors' contributions**

623 BSHN, PJS, and GT designed the experiments. BSHN and PJS performed the experiments with the
624 contribution of NH, RC, and SYL. BSHN performed the experiments related to Fig. 1-3; 4a-c; 5a; S1-
625 S3. PJS performed the experiments related to Fig. 3c-e; Fig. 4a-b; Fig. 5b-e, S2. NH performed the
626 experiments related to Fig. 4d. RC performed the experiments related to Fig. 4a-c, SYL performed the
627 experiments related to Fig. 4a-b. BSHN, PJS, NH, and GT contributed to the writing of the manuscript
628 and the interpretation of the data. All authors read and approved the final manuscript.

629

630 **Acknowledgements**

631 We are grateful to Dr. Davis Ng for providing reagents. We thank Dr. Stefan Kreft for generously
632 providing the plasmids STK05-8-5 and STK05-5-9 [54], Yee Lin Ang and Charlie Marvalim for
633 assisting in cloning. We thank Chengchao Xu and members of Thibault lab for critical reading of the
634 manuscript.

635

636

637

638

639

640

641

642

643

644

645

646

647

648

649

650

651

REFERENCES

1. van Meer G, Voelker DR, Feigenson GW: **Membrane lipids: where they are and how they behave**. *Nat Rev Mol Cell Biol* 2008, **9**(2):112-124.
2. Arendt BM, Ma DW, Simons B, Noureldin SA, Therapondos G, Guindi M, Sherman M, Allard JP: **Nonalcoholic fatty liver disease is associated with lower hepatic and erythrocyte ratios of phosphatidylcholine to phosphatidylethanolamine**. *Applied physiology, nutrition, and metabolism = Physiologie appliquee, nutrition et metabolisme* 2013, **38**(3):334-340.
3. Buang Y, Wang YM, Cha JY, Nagao K, Yanagita T: **Dietary phosphatidylcholine alleviates fatty liver induced by orotic acid**. *Nutrition* 2005, **21**(7-8):867-873.
4. Corbin KD, Zeisel SH: **Choline metabolism provides novel insights into nonalcoholic fatty liver disease and its progression**. *Current opinion in gastroenterology* 2012, **28**(2):159-165.
5. Li Z, Agellon LB, Allen TM, Umeda M, Jewell L, Mason A, Vance DE: **The ratio of phosphatidylcholine to phosphatidylethanolamine influences membrane integrity and steatohepatitis**. *Cell metabolism* 2006, **3**(5):321-331.
6. Kim YJ, Lee HS, Kim YK, Park S, Kim JM, Yun JH, Yu HY, Kim BJ: **Association of Metabolites with Obesity and Type 2 Diabetes Based on FTO Genotype**. *PloS one* 2016, **11**(6):e0156612.
7. Mitsuhashi S, Nishino I: **Phospholipid synthetic defect and mitophagy in muscle disease**. *Autophagy* 2011, **7**(12):1559-1561.
8. Vance DE: **Phospholipid methylation in mammals: from biochemistry to physiological function**. *Biochimica et biophysica acta* 2014, **1838**(6):1477-1487.
9. Fu S, Yang L, Li P, Hofmann O, Dicker L, Hide W, Lin X, Watkins SM, Ivanov AR, Hotamisligil GS: **Aberrant lipid metabolism disrupts calcium homeostasis causing liver endoplasmic reticulum stress in obesity**. *Nature* 2011, **473**(7348):528-531.
10. Jacobs RL, Zhao Y, Koonen DP, Sletten T, Su B, Lingrell S, Cao G, Peake DA, Kuo MS, Proctor SD *et al*: **Impaired de novo choline synthesis explains why phosphatidylethanolamine N-methyltransferase-deficient mice are protected from diet-induced obesity**. *The Journal of biological chemistry* 2010, **285**(29):22403-22413.

11. Dumas ME, Barton RH, Toye A, Cloarec O, Blancher C, Rothwell A, Fearnside J, Tatoud R, Blanc V, Lindon JC *et al*: **Metabolic profiling reveals a contribution of gut microbiota to fatty liver phenotype in insulin-resistant mice**. *Proceedings of the National Academy of Sciences of the United States of America* 2006, **103**(33):12511-12516.

12. Nicholson JK, Holmes E, Kinross J, Burcelin R, Gibson G, Jia W, Pettersson S: **Host-gut microbiota metabolic interactions**. *Science* 2012, **336**(6086):1262-1267.

13. Thibault G, Shui G, Kim W, McAlister GC, Ismail N, Gygi SP, Wenk MR, Ng DT: **The membrane stress response buffers lethal effects of lipid disequilibrium by reprogramming the protein homeostasis network**. *Mol Cell* 2012, **48**(1):16-27.

14. Cox JS, Shamu CE, Walter P: **Transcriptional Induction of Genes Encoding Endoplasmic-Reticulum Resident Proteins Requires a Transmembrane Protein-Kinase**. *Cell* 1993, **73**(6):1197-1206.

15. Travers KJ, Patil CK, Wodicka L, Lockhart DJ, Weissman JS, Walter P: **Functional and genomic analyses reveal an essential coordination between the unfolded protein response and ER-associated degradation**. *Cell* 2000, **101**(3):249-258.

16. Thibault G, Ismail N, Ng DT: **The unfolded protein response supports cellular robustness as a broad-spectrum compensatory pathway**. *Proceedings of the National Academy of Sciences of the United States of America* 2011, **108**(51):20597-20602.

17. Harding HP, Zhang Y, Ron D: **Protein translation and folding are coupled by an endoplasmic-reticulum-resident kinase**. *Nature* 1999, **397**(6716):271-274.

18. Volmer R, Ron D: **Lipid-dependent regulation of the unfolded protein response**. *Current opinion in cell biology* 2015, **33**:67-73.

19. Costanzo M, Baryshnikova A, Bellay J, Kim Y, Spear ED, Sevier CS, Ding H, Koh JL, Toufighi K, Mostafavi S *et al*: **The genetic landscape of a cell**. *Science* 2010, **327**(5964):425-431.

20. Schuldiner M, Collins SR, Thompson NJ, Denic V, Bhamidipati A, Punna T, Ihmels J, Andrews B, Boone C, Greenblatt JF *et al*: **Exploration of the function and organization of the yeast early secretory pathway through an epistatic miniarray profile**. *Cell* 2005, **123**(3):507-519.

21. Jonikas MC, Collins SR, Denic V, Oh E, Quan EM, Schmid V, Weibezahn J, Schwappach B, Walter P, Weissman JS *et al*: **Comprehensive characterization of genes required for protein folding in the endoplasmic reticulum**. *Science* 2009, **323**(5922):1693-1697.

22. Promlek T, Ishiwata-Kimata Y, Shido M, Sakuramoto M, Kohno K, Kimata Y: **Membrane aberrancy and unfolded proteins activate the endoplasmic reticulum stress sensor Ire1 in different ways**. *Molecular biology of the cell* 2011, **22**(18):3520-3532.

23. Volmer R, van der Ploeg K, Ron D: **Membrane lipid saturation activates endoplasmic reticulum unfolded protein response transducers through their transmembrane domains**. *Proceedings of the National Academy of Sciences of the United States of America* 2013, **110**(12):4628-4633.

24. Wu H, Ng BS, Thibault G: **Endoplasmic reticulum stress response in yeast and humans**. *Biosci Rep* 2014, **34**(4).

25. Yang L, Zhao D, Ren J, Yang J: **Endoplasmic reticulum stress and protein quality control in diabetic cardiomyopathy**. *Biochimica et biophysica acta* 2015, **1852**(2):209-218.

26. Pagliassotti MJ: **Endoplasmic reticulum stress in nonalcoholic fatty liver disease**. *Annu Rev Nutr* 2012, **32**:17-33.

27. Biederer T, Volkwein C, Sommer T: **Role of Cue1p in ubiquitination and degradation at the ER surface**. *Science* 1997, **278**(5344):1806-1809.

28. Shurtleff MJ, Itzhak DN, Hussmann JA, Schirle Oakdale NT, Costa EA, Jonikas M, Weibezahn J, Popova KD, Jan CH, Sinitcyn P *et al*: **The ER membrane protein complex interacts cotranslationally to enable biogenesis of multipass membrane proteins**. *Elife* 2018, **7**.

29. Lahiri S, Chao JT, Tavassoli S, Wong AK, Choudhary V, Young BP, Loewen CJ, Prinz WA: **A conserved endoplasmic reticulum membrane protein complex (EMC) facilitates phospholipid transfer from the ER to mitochondria**. *PLoS Biol* 2014, **12**(10):e1001969.

30. Flury I, Garza R, Shearer A, Rosen J, Cronin S, Hampton RY: **INSIG: a broadly conserved transmembrane chaperone for sterol-sensing domain proteins**. *The EMBO journal* 2005, **24**(22):3917-3926.

31. Shao S, Hegde RS: **Membrane protein insertion at the endoplasmic reticulum**. *Annu Rev Cell Dev Biol* 2011, **27**:25-56.

32. Park E, Rapoport TA: **Mechanisms of Sec61/SecY-mediated protein translocation across membranes**. *Annu Rev Biophys* 2012, **41**:21-40.

33. Mandon EC, Trueman SF, Gilmore R: **Protein translocation across the rough endoplasmic reticulum**. *Cold Spring Harb Perspect Biol* 2013, **5**(2).

34. Feng D, Zhao X, Soromani C, Toikkanen J, Romisch K, Vembar SS, Brodsky JL, Keranen S, Jantti J: **The transmembrane domain is sufficient for Sbh1p function, its association with the Sec61 complex, and interaction with Rtn1p**. *The Journal of biological chemistry* 2007, **282**(42):30618-30628.

35. Wang F, Whynot A, Tung M, Denic V: **The mechanism of tail-anchored protein insertion into the ER membrane**. *Mol Cell* 2011, **43**(5):738-750.

36. Carman GM, Henry SA: **Phospholipid biosynthesis in yeast**. *Annual review of biochemistry* 1989, **58**:635-669.

37. Vevea JD, Garcia EJ, Chan RB, Zhou B, Schultz M, Di Paolo G, McCaffery JM, Pon LA: **Role for Lipid Droplet Biogenesis and Microlipophagy in Adaptation to Lipid Imbalance in Yeast**. *Dev Cell* 2015, **35**(5):584-599.

38. Chapman RE, Walter P: **Translational attenuation mediated by an mRNA intron**. *Curr Biol* 1997, **7**(11):850-859.

39. Vance JE, Tasseva G: **Formation and function of phosphatidylserine and phosphatidylethanolamine in mammalian cells**. *Biochimica et biophysica acta* 2013, **1831**(3):543-554.

40. Boumann HA, Gubbens J, Koorengevel MC, Oh CS, Martin CE, Heck AJ, Patton-Vogt J, Henry SA, de Kruijff B, de Kroon AI: **Depletion of phosphatidylcholine in yeast induces shortening and increased saturation of the lipid acyl chains: evidence for regulation of intrinsic membrane curvature in a eukaryote**. *Molecular biology of the cell* 2006, **17**(2):1006-1017.

41. Zimmerberg J, Kozlov MM: **How proteins produce cellular membrane curvature**. *Nat Rev Mol Cell Bio* 2006, **7**(1):9-19.

42. Quinn PJ: **The fluidity of cell membranes and its regulation**. *Progress in biophysics and molecular biology* 1981, **38**(1):1-104.

43. Stubbs CD: **Membrane fluidity: structure and dynamics of membrane lipids**. *Essays in biochemistry* 1983, **19**:1-39.

44. Stubbs CD, Smith AD: **The modification of mammalian membrane polyunsaturated fatty acid composition in relation to membrane fluidity and function**. *Biochimica et biophysica acta* 1984, **779**(1):89-137.

45. Shibata Y, Voss C, Rist JM, Hu J, Rapoport TA, Prinz WA, Voeltz GK: **The reticulon and DP1/Yop1p proteins form immobile oligomers in the tubular endoplasmic reticulum**. *The Journal of biological chemistry* 2008, **283**(27):18892-18904.

46. Dawaliby R, Trubbia C, Delporte C, Noyon C, Ruysschaert JM, Van Antwerpen P, Govaerts C: **Phosphatidylethanolamine Is a Key Regulator of Membrane Fluidity in Eukaryotic Cells**. *Journal of Biological Chemistry* 2016, **291**(7):3658-3667.

47. Snider J, Kittanakom S, Damjanovic D, Curak J, Wong V, Stagljar I: **Detecting interactions with membrane proteins using a membrane two-hybrid assay in yeast**. *Nat Protoc* 2010, **5**(7):1281-1293.

48. Paumi CM, Menendez J, Arnoldo A, Engels K, Iyer KR, Thaminy S, Georgiev O, Barral Y, Michaelis S, Stagljar I: **Mapping protein-protein interactions for the yeast ABC transporter Ycf1p by integrated split-ubiquitin membrane yeast two-hybrid analysis**. *Mol Cell* 2007, **26**(1):15-25.

49. Snider J, Kittanakom S, Curak J, Stagljar I: **Split-ubiquitin based membrane yeast two-hybrid (MYTH) system: a powerful tool for identifying protein-protein interactions**. *Journal of visualized experiments : JoVE* 2010(36).

50. Chavan M, Yan A, Lennarz WJ: **Subunits of the translocon interact with components of the oligosaccharyl transferase complex**. *The Journal of biological chemistry* 2005, **280**(24):22917-22924.

51. Panzner S, Dreier L, Hartmann E, Kostka S, Rapoport TA: **Posttranslational protein transport in yeast reconstituted with a purified complex of Sec proteins and Kar2p**. *Cell* 1995, **81**(4):561-570.

52. Babu M, Vlasblom J, Pu S, Guo X, Graham C, Bean BD, Burston HE, Vizeacoumar FJ, Snider J, Phanse S *et al*: **Interaction landscape of membrane-protein complexes in Saccharomyces cerevisiae**. *Nature* 2012, **489**(7417):585-589.

53. Zhao X, Jantti J: **Functional characterization of the trans-membrane domain interactions of the Sec61 protein translocation complex beta-subunit**. *BMC Cell Biol* 2009, **10**:76.

54. Habeck G, Ebner FA, Shimada-Kreft H, Kreft SG: **The yeast ERAD-C ubiquitin ligase Doa10 recognizes an intramembrane degron**. *The Journal of cell biology* 2015, **209**(4):621.

55. Carvalho P, Goder V, Rapoport TA: **Distinct ubiquitin-ligase complexes define convergent pathways for the degradation of ER proteins**. *Cell* 2006, **126**(2):361-373.

56. Deng M, Hochstrasser M: **Spatially regulated ubiquitin ligation by an ER/nuclear membrane ligase**. *Nature* 2006, **443**(7113):827-831.

57. Vashist S, Ng DT: **Misfolded proteins are sorted by a sequential checkpoint mechanism of ER quality control**. *The Journal of cell biology* 2004, **165**(1):41-52.

58. Ye YH, Meyer HH, Rapoport TA: **The AAA ATPase Cdc48/p97 and its partners transport proteins from the ER into the cytosol**. *Nature* 2001, **414**(6864):652-656.

59. Braun S, Matuschewski K, Rape M, Thoms S, Jentsch S: **Role of the ubiquitin-selective CDC48(UFD1/NPL4)chaperone (segregase) in ERAD of OLE1 and other substrates**. *The EMBO journal* 2002, **21**(4):615-621.

60. Suzuki T, Park H, Hollingsworth NM, Sternglanz R, Lennarz WJ: **PNG1, a yeast gene encoding a highly conserved peptide:N-glycanase**. *The Journal of cell biology* 2000, **149**(5):1039-1052.

61. Thibault G, Ng DT: **The endoplasmic reticulum-associated degradation pathways of budding yeast**. *Cold Spring Harb Perspect Biol* 2012, **4**(12).

62. Swanson R, Locher M, Hochstrasser M: **A conserved ubiquitin ligase of the nuclear envelope/endoplasmic reticulum that functions in both ER-associated and Matalpha2 repressor degradation**. *Genes & development* 2001, **15**(20):2660-2674.

63. Hirsch C, Gauss R, Horn SC, Neuber O, Sommer T: **The ubiquitylation machinery of the endoplasmic reticulum**. *Nature* 2009, **458**(7237):453-460.

64. Brodsky JL, Skach WR: **Protein folding and quality control in the endoplasmic reticulum: Recent lessons from yeast and mammalian cell systems**. *Current opinion in cell biology* 2011, **23**(4):464-475.

65. Finley D, Ulrich HD, Sommer T, Kaiser P: **The ubiquitin-proteasome system of Saccharomyces cerevisiae**. *Genetics* 2012, **192**(2):319-360.

828 66. Rubenstein EM, Kreft SG, Greenblatt W, Swanson R, Hochstrasser M: **Aberrant substrate**
829 **engagement of the ER translocon triggers degradation by the Hrd1 ubiquitin ligase**.
830 *The Journal of cell biology* 2012, **197**(6):761-773.
831 67. Christianson JC, Ye Y: **Cleaning up in the endoplasmic reticulum: ubiquitin in charge**.
832 *Nat Struct Mol Biol* 2014, **21**(4):325-335.
833 68. Ruggiano A, Foresti O, Carvalho P: **Quality control: ER-associated degradation: protein**
834 **quality control and beyond**. *The Journal of cell biology* 2014, **204**(6):869-879.
835 69. Zattas D, Hochstrasser M: **Ubiquitin-dependent protein degradation at the yeast**
836 **endoplasmic reticulum and nuclear envelope**. *Crit Rev Biochem Mol Biol* 2015, **50**(1):1-17.
837 70. Malhotra N, Beaton MD: **Management of non-alcoholic fatty liver disease in 2015**. *World J*
838 *Hepatol* 2015, **7**(30):2962-2967.
839 71. Doycheva I, Watt KD, Rifai G, Abou Mrad R, Lopez R, Zein NN, Carey WD, Alkhouri N:
840 **Increasing Burden of Chronic Liver Disease Among Adolescents and Young Adults in**
841 **the USA: A Silent Epidemic**. *Dig Dis Sci* 2017, **62**(5):1373-1380.
842 72. Puri P, Baillie RA, Wiest MM, Mirshahi F, Choudhury J, Cheung O, Sargeant C, Contos MJ,
843 Sanyal AJ: **A lipidomic analysis of nonalcoholic fatty liver disease**. *Hepatology* 2007,
844 **46**(4):1081-1090.
845 73. Wattacheril J, Seeley EH, Angel P, Chen H, Bowen BP, Lanciault C, Caprioli RM, Abumrad N,
846 Flynn CR: **Differential intrahepatic phospholipid zonation in simple steatosis and**
847 **nonalcoholic steatohepatitis**. *PloS one* 2013, **8**(2):e57165.
848 74. Puri P, Mirshahi F, Cheung O, Natarajan R, Maher JW, Kellum JM, Sanyal AJ: **Activation**
849 **and dysregulation of the unfolded protein response in nonalcoholic fatty liver disease**.
850 *Gastroenterology* 2008, **134**(2):568-576.
851 75. Yang L, Li P, Fu S, Calay ES, Hotamisligil GS: **Defective hepatic autophagy in obesity**
852 **promotes ER stress and causes insulin resistance**. *Cell metabolism* 2010, **11**(6):467-478.
853 76. Szule JA, Fuller NL, Rand RP: **The effects of acyl chain length and saturation of**
854 **diacylglycerols and phosphatidylcholines on membrane monolayer curvature**.
855 *Biophysical journal* 2002, **83**(2):977-984.

77. Zinser E, Paltauf F, Daum G: **Sterol composition of yeast organelle membranes and subcellular distribution of enzymes involved in sterol metabolism**. *Journal of bacteriology* 1993, **175**(10):2853-2858.

78. Mansilla MC, Cybulski LE, Albanesi D, de Mendoza D: **Control of membrane lipid fluidity by molecular thermosensors**. *Journal of bacteriology* 2004, **186**(20):6681-6688.

79. Pineau L, Bonifait L, Berjeaud JM, Alimardani-Theuil P, Berges T, Ferreira T: **A lipid-mediated quality control process in the Golgi apparatus in yeast**. *Molecular biology of the cell* 2008, **19**(3):807-821.

80. Holthuis JC, Menon AK: **Lipid landscapes and pipelines in membrane homeostasis**. *Nature* 2014, **510**(7503):48-57.

81. Boban M, Ljungdahl PO, Foisner R: **Atypical ubiquitylation in yeast targets lysine-less Asi2 for proteasomal degradation**. *The Journal of biological chemistry* 2015, **290**(4):2489-2495.

82. Lauwers E, Grossmann G, Andre B: **Evidence for coupled biogenesis of yeast Gap1 permease and sphingolipids: essential role in transport activity and normal control by ubiquitination**. *Molecular biology of the cell* 2007, **18**(8):3068-3080.

83. Payet LA, Pineau L, Snyder EC, Colas J, Moussa A, Vannier B, Bigay J, Clarhaut J, Becq F, Berjeaud JM *et al*: **Saturated fatty acids alter the late secretory pathway by modulating membrane properties**. *Traffic* 2013, **14**(12):1228-1241.

84. Babst M: **Quality control: quality control at the plasma membrane: one mechanism does not fit all**. *The Journal of cell biology* 2014, **205**(1):11-20.

85. Ginsberg BH, Brown TJ, Simon I, Spector AA: **Effect of the membrane lipid environment on the properties of insulin receptors**. *Diabetes* 1981, **30**(9):773-780.

86. Malhi H, Kaufman RJ: **Endoplasmic reticulum stress in liver disease**. *J Hepatol* 2011, **54**(4):795-809.

87. Bobenchik AM, Choi JY, Mishra A, Rujan IN, Hao B, Voelker DR, Hoch JC, Ben Mamoun C: **Identification of inhibitors of Plasmodium falciparum phosphoethanolamine methyltransferase using an enzyme-coupled transmethylation assay**. *Bmc Biochem* 2010, **11**.

885 88. Holz GG, Jr.: **Lipids and the malarial parasite**. *Bull World Health Organ* 1977, **55**(2-3):237-
886 248.
887 89. Pessi G, Ben Mamoun C: **Pathways for phosphatidylcholine biosynthesis: targets and**
888 **strategies for antimalarial drugs**. *Future Lipidol* 2006, **1**(2):173-180.
889 90. Mok S, Ashley EA, Ferreira PE, Zhu L, Lin Z, Yeo T, Chotivanich K, Imwong M,
890 Pukrittayakamee S, Dhorda M *et al*: **Drug resistance. Population transcriptomics of**
891 **human malaria parasites reveals the mechanism of artemisinin resistance**. *Science*
892 2015, **347**(6220):431-435.
893 91. Ben Mamoun C, Prigge ST, Vial H: **Targeting the Lipid Metabolic Pathways for the**
894 **Treatment of Malaria**. *Drug Dev Res* 2010, **71**(1):44-55.
895 92. Bi M, Naczki C, Koritzinsky M, Fels D, Blais J, Hu N, Harding H, Novoa I, Varia M, Raleigh J
896 *et al*: **ER stress-regulated translation increases tolerance to extreme hypoxia and**
897 **promotes tumor growth**. *The EMBO journal* 2005, **24**(19):3470-3481.
898 93. Nelson DR, Lawson JE, Klingenberg M, Douglas MG: **Site-directed mutagenesis of the**
899 **yeast mitochondrial ADP/ATP translocator. Six arginines and one lysine are essential**.
900 *J Mol Biol* 1993, **230**(4):1159-1170.
901 94. Prasad R, Kawaguchi S, Ng DT: **A nucleus-based quality control mechanism for**
902 **cytosolic proteins**. *Molecular biology of the cell* 2010, **21**(13):2117-2127.
903 95. Spear ED, Ng DT: **Stress tolerance of misfolded carboxypeptidase Y requires**
904 **maintenance of protein trafficking and degradative pathways**. *Molecular biology of the*
905 *cell* 2003, **14**(7):2756-2767.
906 96. Wang S, Thibault G, Ng DT: **Routing misfolded proteins through the multivesicular body**
907 **(MVB) pathway protects against proteotoxicity**. *The Journal of biological chemistry* 2011,
908 **286**(33):29376-29387.
909 97. Day CA, Kraft LJ, Kang M, Kenworthy AK: **Analysis of protein and lipid dynamics using**
910 **confocal fluorescence recovery after photobleaching (FRAP)**. *Curr Protoc Cytom* 2012,
911 **Chapter 2**:Unit2 19.
912 98. Feder TJ, Brust-Mascher I, Slattery JP, Baird B, Webb WW: **Constrained diffusion or**
913 **immobile fraction on cell surfaces: a new interpretation**. *Biophysical journal* 1996,
914 **70**(6):2767-2773.

99. Biederer T, Volkwein C, Sommer T: **Degradation of subunits of the Sec61p complex, an integral component of the ER membrane, by the ubiquitin-proteasome pathway**. *The EMBO journal* 1996, **15**(9):2069-2076.

FIGURE LEGENDS

Figure 1. A subset of ER transmembrane proteins is prematurely degraded under lipid imbalance.

(**a**) Metabolic pathways for the synthesis of phosphatidylcholine in *S. cerevisiae*. PE, phosphatidylethanolamine; MMPE, *N*-monomethyl phosphatidylethanolamine; DMPE, *N*,*N*-dimethyl phosphatidylethanolamine; PC, phosphatidylcholine; DAG, diacylglycerol; CDP-choline, cytidine diphosphate-choline; P-choline, phosphate-choline. (**b**) Steady state level of transmembrane proteins. Equal cell numbers were harvested. Proteins were separated by SDS-PAGE and detected by immunoblotting with antibodies against the HA tag and Tub1 as loading control. $^{a}P<0.05$, $^{b}P<0.01$, $^{c}P<0.005$, Student's t test. (**c**) Degradation of HA-tagged proteins was analysed after blocking protein translation with cycloheximide. Proteins were separated by SDS-PAGE and detected by immunoblotting with antibodies against the HA tag and Pgk1 as loading control.

Figure 2. Transmembrane proteins are destabilised by the decrease in phosphatidylcholine synthesis.

(**a**) Protein candidates were detected using antibodies against HA tag and Kar2 as ER marker. Scale bar, 5 µm. (**b**) Membranes prepared from wild type and *opi3*Δ cells expressing HA-tagged proteins were treated with 0.1 M sodium carbonate, pH 11, for 30 min on ice. A portion was kept as the total fraction (T), and the remaining was subjected to centrifugation at 100,000 X *g*. Supernatant (S) and membrane pellet (P) fractions were collected and analysed by immunoblotting. Proteins were detected using anti-HA antibody. Kar2 and Sec61 serve as soluble and integral membrane protein controls, respectively. (**c**) Membranes prepared from WT and *opi3*Δ cells expressing HA-tagged proteins were treated with 1 mg/ml proteinase K, for 30 min at 37°C, with or without 1% NP40. HA-tagged proteins were precipitated with 10% TCA, separated by SDS-PAGE and detected by immunoblotting with HA antibody. Expected protein molecular weights are shown below for non-digested (N), digested (D), and flipped and digested (F). The orientation of the HA tag is shown as black dot. Fragments missing the HA tag and are therefore undetectable are illustrated with transparency. The ER lumen and cytosol are at the top and bottom of the membrane, respectively.

Figure 3. Sbh1 is destabilised from increased membrane fluidity of the ER membrane.

(**a**) Cell were grown with or without 1 mM choline before addition of cycloheximide. Time points were taken as indicated. Proteins were separated by SDS-PAGE and detected by immunoblotting with antibodies against the HA tag and Tub1 as loading control. (**b**) Heat map of log_2-transformed fold changes (FC) in fatty acids (FA) in *opi3*Δ as compared to WT. FAs in whole cells and microsomes (ER) of WT and *opi3*Δ were quantified by gas chromatography after FAME derivatisation. (**c-e**) Fluorescence recovery after photobleaching using Sec63-sGFP in WT and *opi3*Δ. (**c**) Averages of Sec63-sGFP signal intensity from 20 cells are plotted over a 60-second period. (**d**) Fluorescence intensity was monitored from the white boxes ROI (region of interest), REF (reference), and BG (background). Scale bar, 5 µm. A region of the cortical ER of live cells were photobleached and recovery points at 1.57 s intervals were taken. (**e**) The time elapsed for the half-maximal fluorescence recovery ($t_{½}$) was calculated and plotted. Student's t test compared to WT.

Figure 4. Sbh1 binding to interacting parters is compromised under lipid imbalance.

(**a,b**) Proteins identified as interacting partners of N-termini reporter tagged Sbh1 (TF-C_{ub}-Sbh1) by the MYTH method in WT (A) and *opi3*Δ (B) cells. ERAD factors were only detected in *opi3*Δ and are denoted in red. Previously reported interactors of Sbh1 are indicated with black dots. (**c**) The degradation of Sec61 or Sss1-Flag was analysed in WT and *opi3*Δ cells after blocking translation with cycloheximide. Proteins were separated by SDS-PAGE and detected by immunoblotting with antibodies against Sec61 or Flag tag and Tub1 as loading control. (**d**) Immunoprecipitation of Sbh1-HA with protein G beads were analysed in WT and *opi3*Δ native cell lysates. Eluted and input fractions were resolved by SDS-PAGE, transferred to nitrocellulose membrane, and analysed by immunoblotting with antibodies against Sec61 and the HA tag after the release of HA bound Sbh1 with HA peptide.

Figure 5. Sbh1 is destabilised from its transmembrane domain and degraded in a Doa10-dependent manner.

(**a**) The degradation of Sbh1-HA was analysed in WT, *opi3*Δ, *opi3*Δ*doa10*Δ, *opi3*Δ*hrd1*Δ, and *opi3*Δ*usa1*Δ cells after blocking translation with cycloheximide. Proteins were separated by SDS-PAGE and detected by immunoblotting with antibodies against the HA tag and Tub1 as loading

control. (**b**) The degradation of Sbh1-HA in WT and *opi3*Δ cells or Sbh1 cytosolic lysine mutant in *opi3*Δ cells treated as in **a**. (**c**) Sbh1 percentage remaining at the 60 min time point from **b**. (**d**) The degradation of Sbh1-HA in WT and *opi3*Δ cells or Sbh1 all cytosolic lysine mutated to alanine [Sbh1(6KA)] in *opi3*Δ cells treated as in **a**. (**e**) Sbh1 percentage remaining at the 60 min time point from **d**. (**f**) The degradation of mutant Sbh2 with amino acids 61 and 68 mutated to proline and alanine, respectively [HA-Sbh2(S61P,S68A)], and chimeric Sbh1 protein with its transmembrane domain replaced with that of Sbh2 (HA-Sbh121) in WT and *opi3*Δ cells treated as in **a**. The ER lumen and cytosol are at the top and bottom of the membrane, respectively.

Figure 6. Premature degradation of TPs leads to chronic ER stress and development of NAFLD.

Normally, ER homeostasis can be reached from lipid perturbation through the regulation of downstream UPR target genes. UPR transactivator (yellow protein representing Ire1, PERK, or ATF6) senses ER stress from the accumulation of misfolded proteins and/or lipid perturbation. However, under prolonged LP, ER homeostasis could not be achieved due to the premature degradation of a subset of misfolded proteins (blue protein) leading to chronic ER stress, cell death, and eventually the development of NAFLD.

ADDITIONAL FILES

Additional file 1: Supplemental methods and data, **Figures S1-S3**, and **Tables S2-S4.** (PDF file)

Additional file 2: Table S1. List of genes upregulated transcriptionally but having lower protein abundance under LP. (XLSX file)

SUPPLEMENTARY FIGURE LEGEND

Figure S1. Strong activation of the UPR does not destabilise Sbh1.

(**a**) The degradation of Sbh1-HA was analysed in WT and *opi3*Δ cells containing control vector (ve) or *HAC1*^{i}-bearing plasmid after blocking translation with cycloheximide. Proteins were separated by SDS-PAGE and detected by immunoblotting with antibodies against the HA tag and Tub1 as loading control. (**b**) Cells were grown to early log phase at 30˚C in selective synthetic complete media. UPR induction was measured using a *UPRE-LacZ* reporter assay. Tm, tunicamycin.

Figure S2. Validation of Sbh1 interacting partners.

(**a**) N-termini reporter tagged Sbh1 (TF-C_{ub}-Sbh1) remains localised to the ER membrane in both WT and *opi3*Δ. Protein candidates were detected using antibodies against LexA and eroGFP as ER marker. Scale bar, 5 µm. (**b**) Interacting proteins of N-tagged (TF-C_{ub}-Sbh1) were retransformed with the original bait strain, together with a negative control using the single-pass transmembrane domain of human T-cell surface glycoprotein CD4 tagged to C_{ub}-LexA-VP16 MYTH. Positive control of pOST1-N_{ub}I bait was used (ve ctrl). Tm, tunicamycin.

Figure S3. Sbh1 is degraded by the ERAD and not the vacuolar pathways.

The degradation of Sbh1-HA was analysed in WT, *opi3*Δ, *opi3*Δ*cue1*Δ, and *opi3*Δ*pep4*Δ cells after blocking translation with cycloheximide. Proteins were separated by SDS-PAGE and detected by immunoblotting with antibodies against the HA tag and PGK1 as loading control.

1066 **Table S2. Strains used in the study**

Strains	Genotype	Source
W303a	*MAT*a, *leu2-3,112, his3-11, trp1-1, ura3-1, can1-100, ade2-1*	[14]
GTY68	*MATa, opi3::KANMX,* W303 background	[13]
YGT0315	*MAT*a, pGT0181, W303 background	This study
YGT0317	*MAT*a, *opi3::KANMX*, pGT0181, W303 background	This study
YGT0318	*MAT*a, pGT0182, W303 background	This study
YGT0320	*MAT*a, *opi3::KANMX*, pGT0182, W303 background	This study
YGT0321	*MAT*a, pGT0179, W303 background	This study
YGT0323	*MAT*a, *opi3::KANMX*, pGT0179, W303 background	This study
YGT0327	*MAT*a, pGT0185, W303 background	This study
YGT0329	*MAT*a, *opi3::KANMX*, pGT0185, W303 background	This study
YGT0330	*MAT*a, pGT0315, W303 background	This study
YGT0332	*MAT*a, *opi3::KANMX*, pGT0315, W303 background	This study
YGT0374	*MAT*a, pGT0183, W303 background	This study
YGT0375	*MAT*a, *opi3::KANMX*, pGT0183, W303 background	This study
YGT0432	*MAT*a, pJC835, W303 background	This study
YGT0540	*MAT*a, pGT0288, NMY51 background (*his3Δ200*, *trp-901*, *leu2-3,112*, *ade2*, *LYS::(lexAop)4-HIS3*, *ura3::(lexAop)8-LACZ*, *(lexAop)8-ADE2*, *GAL4*)	This study
YGT0541	MATa, *opi3::KANMX*, pGT0183, NMY51 background	This study
YGT0574	*MAT*a, *doa10::KANMX*, *opi3::KANMX*, pGT0183, W303 background	This study
YGT0575	*MAT*a, *hrd1::KANMX*, *opi3::KANMX*, pGT0183, W303 background	This study
YGT0576	*MAT*a, *usa11::KANMX*, *opi3::KANMX*, pGT0183, W303 background	This study
YGT0671	*MAT*a, pGT0352, W303 background	This study
YGT0672	*MAT*a, *opi3::KANMX*, pGT0352, W303 background	This study
YGT0673	*MAT*a, pGT0183, pRS313, W303 background	This study
YGT0674	*MAT*a, *opi3::KANMX*, pGT0183, pRS313, W303 background	This study
YGT0675	*MAT*a, pGT0183, pGT0349, W303 background	This study
YGT0676	*MAT*a, *opi3::KANMX*, pGT0183, pGT0349, W303 background	This study
YGT0690	*MAT*a, pGT0180 , W303 background	This study
YGT0691	*MAT*a, *opi3::KANMX*, pGT0180, W303 background	This study
YGT0721	*MAT*a, pGT0350, pGT0183, W303 background	This study
YGT0722	*MAT*a, *opi3::KANMX*, pGT0350, pGT0183, W303 background	This study
YGT0725	*MAT*a, pGT0350, pRS315, W303 background	This study
YGT0726	*MAT*a, *opi3::KANMX*, pGT0350, pRS315, W303 background	This study
YGT0769	*MAT*a, pGT0366, W303 background	This study
YGT0770	*MAT*a, *opi3::KANMX*, pGT0366, W303 background	This study
YGT0771	*MAT*a, pGT0368, W303 background	This study
YGT0772	*MAT*a, *opi3::KANMX*, pGT0368, W303 background	This study
YGT0773	*MAT*a, pGT0365, W303 background	This study
YGT0774	*MAT*a, *opi3::KANMX*, pGT0365, W303 background	This study
YGT0874	*MAT*a, pPS1622, pRS313, W303 background	This study
YGT0875	*MAT*a, *opi3::KANMX*, pPS1622, pRS313, W303 background	This study
YGT0876	*MAT*a, pGT0349, pPS1622, W303 background	This study
YGT0877	*MAT*a, *opi3::KANMX*, pGT0349, pPS1622, W303 background	This study
YGT1122	*MAT*a, pGT0445, W303 background	This study
YGT1123	*MAT*a, *opi3::KANMX*, pGT0445, W303 background	This study
YGT1124	*MAT*a, pGT0446, W303 background	This study
YGT1125	*MAT*a, *opi3::KANMX*, pGT0446, W303 background	This study
YGT1126	*MAT*a, pGT0447, W303 background	This study
YGT1127	*MAT*a, *opi3::KANMX*, pGT0447, W303 background	This study
YGT1148	*MAT*a, pGT0459, W303 background	This study
YGT1149	*MAT*a, *opi3::KANMX*, pGT0459, W303 background	This study
YGT1167	*MAT*a, STK05-5-9, W303 background	This study
YGT1168	*MAT*a, *opi3::KANMX*, STK05-5-9, W303 background	This study
YGT1169	*MAT*a, STK05-8-5, W303 background	This study
YGT1170	*MAT*a, *opi3::KANMX*, STK05-8-5, W303 background	This study

Table S3. Plasmids used in the study

Plasmid	Encoded protein	Promoter	Vector	Source
pJC31	β-galactosidase	*UPRC-CYC1*	pRS315	[100]
pPS1622	Sec63-sGFP	*SEC63*	pRS316	[101]
pJC835	Hac1	*HAC1*	pRS313	[14]
pGT0284	IRE1-3X FLAG	*IRE1*	pRS426	[102]
pPM28	eroGFP	*GAP*	pRS316	[103]
STK05-5-9	HA-Sbh2(S61P,S68A)	*MET25*	p413MET25	[104]
STK05-8-5	HA-Sbh121	*MET25*	p413MET25	[104]
pGT0179	Nsg2-HA	*NSG2*	pRS315	This study
pGT0181	Cue1-HA	*CUE1*	pRS315	This study
pGT0183	Sbh1-HA	*SBH1*	pRS315	This study
pGT0185	Emc4-HA	*EMC4*	pRS315	This study
pGT0288	C_{ub}-LexA-VP16-Sbh1	*CYC1*	pBT3-N	This study
pGT0352	Sbh1(K41A)-HA	*SBH1*	pRS315	This study
pGT0350	Sss1-3XFlag	*SSS1*	pRS313	This study
pGT0445	Sbh1(K15/17A)-HA	*SBH1*	pRS315	This study
pGT0446	Sbh1(K23A)-HA	*SBH1*	pRS315	This study
pGT0447	Sbh1(K30/31)-HA	*SBH1*	pRS315	This study
pGT0459	Sbh1(6KA)-HA	*SBH1*	pRS315	This study

Table S4. **Oligonucleotide primers used in the study**

Primer	Sequence (5' to 3')
BN013	CCGCGGTGGCGGCCGCCACTAGCCGATGTTATC
BN014	GTAGTCCGCATGCCCAACAATAACGTATCTGATTGG
BN015	GGGCATGCGGACTACAAAGACCATGACG
BN016	CGGCCGCCACCGCGGTGG
BN027	ATGAGGGCCATTACGGCCATGTCAAGCCCAACTCCTCC
BN028	CTCATGGCCGAGGCGGCCTTAAAATAACTTACCGGCAACTTTAGAAATAACATG
BN029	CTCATGCTGCAGATGGAGGATTCGAGATTGCTTATCACTTTG
BN030	CTCATGCCATGGGAGTCAGCAAACTTTGCAAATCTTTATCAC
BN031	AACGTCGCGGCCGCAGCAAATGATTCCTCGACTGAATATAAAGG
BN032	CCATGGCGCGCTAATCGGAAAACCATTGTAATCCATTATTATAATGAGCA
BN033	CTCATGCTGCAGATGGCCAATAGAGGAGAACCGG
BN034	CTCATGCCATGGGATGAGAATATAGATATCTTCCTAGTTTTCCAAACATTAG
BN035	CTCATGCTGCAGATGTCAAGCCCAACTCCTCC
BN036	CTCATGCCATGGGAAATAACTTACCGGCAACTTTAGAAATAACATG
BN037	AATTCGATTTTGGCGATTTATTCTGAT
BN038	ATTGCTGTTCGTGTTTTTCTTTGGAGC
PS139	TACTTTGCAAGCGAGAGCACAGGGAAGTTC
PS140	CGTTGACCACCTGGAGGAGTTGGG
PS141	AAGTTCACAAGCAGTTGCGGCAT
PS142	CCCTGTTTTCTCTTTTGCAAAGTACG
PS143	ATCCGCTCCAGCGGCAAACACGAACA
PS144	GCCGCAACTTTTTGTGAACTTCCCTGTTTT
PS153	AAAGTTGCGGCATCCGCTC
PS154	TTGTGAACTTCCCTGTGCTCTCGCTTGCAAAG

SUPPLEMENTAL REFERENCES

100. Cox JS, Walter P: **A novel mechanism for regulating activity of a transcription factor that controls the unfolded protein response**. *Cell* 1996, **87**(3):391-404.

101. Prinz WA, Grzyb L, Veenhuis M, Kahana JA, Silver PA, Rapoport TA: **Mutants affecting the structure of the cortical endoplasmic reticulum in Saccharomyces cerevisiae**. *The Journal of cell biology* 2000, **150**(3):461-474.

102. Kimata Y, Oikawa D, Shimizu Y, Ishiwata-Kimata Y, Kohno K: **A role for BiP as an adjustor for the endoplasmic reticulum stress-sensing protein Ire1**. *The Journal of cell biology* 2004, **167**(3):445-456.

103. Merksamer PI, Trusina A, Papa FR: **Real-time redox measurements during endoplasmic reticulum stress reveal interlinked protein folding functions**. *Cell* 2008, **135**(5):933-947.

104. Habeck G, Ebner FA, Shimada-Kreft H, Kreft SG: **The yeast ERAD-C ubiquitin ligase Doa10 recognizes an intramembrane degron**. *The Journal of cell biology* 2015, **209**(2):261-273.

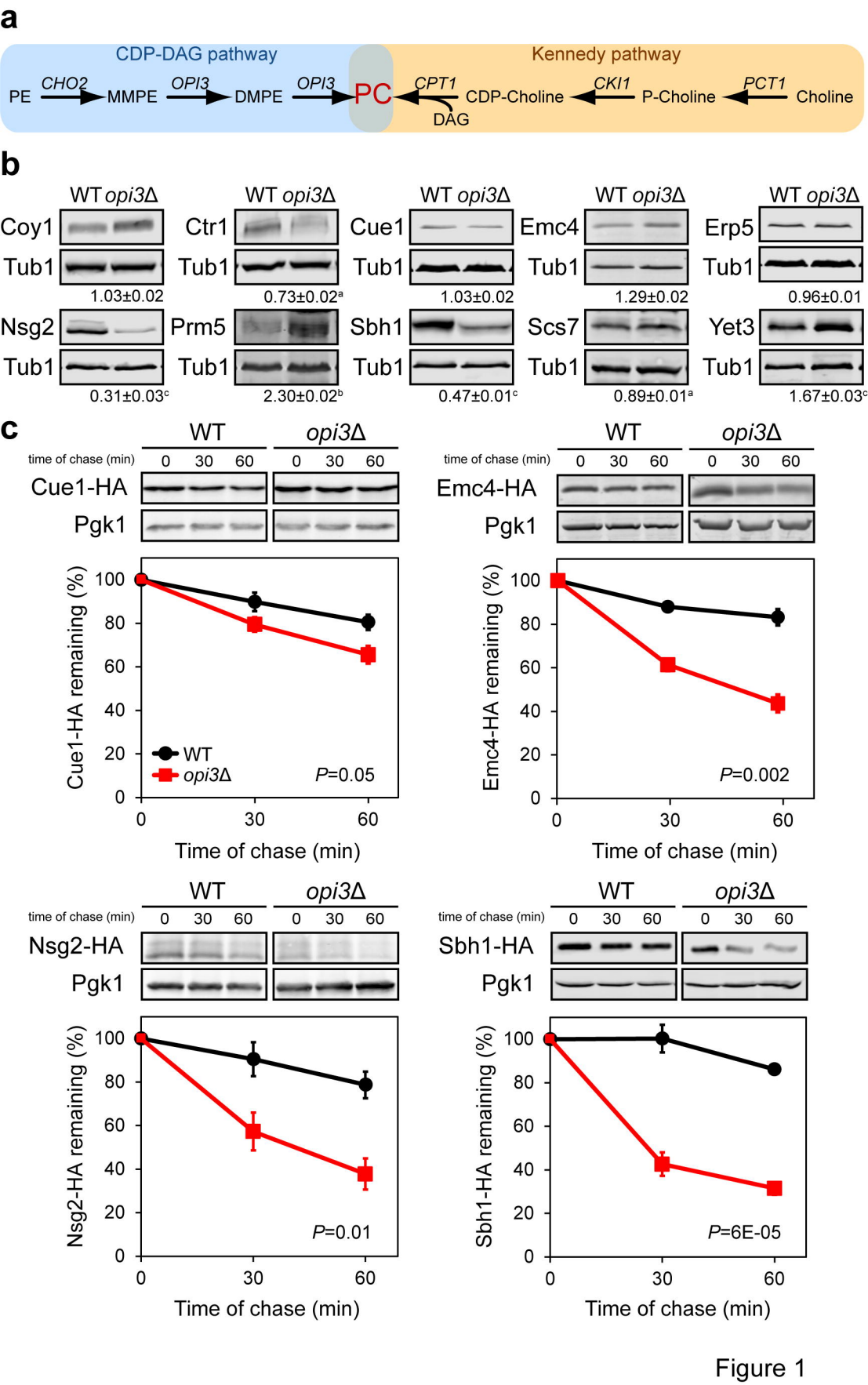
a
CDP-DAG pathway
Kennedy pathway
PE
CHO2
MMPE
OPI3
DMPE
OPI3
PC
CPT1
CDP-Choline
CKI1
P-Choline
PCT1
Choline
DAG
b
WT opi3Δ
Coy1
Tub1
1.03±0.02
Ctr1
Tub1
0.73±0.02a
Cue1
Tub1
1.03±0.02
Emc4
Tub1
1.29±0.02
Erp5
Tub1
0.96±0.01
Nsg2
Tub1
0.31±0.03c
Prm5
Tub1
2.30±0.02b
Sbh1
Tub1
0.47±0.01c
Scs7
Tub1
0.89±0.01a
Yet3
Tub1
1.67±0.03c
c
WT
opi3Δ
time of chase (min)
0 30 60 0 30 60
Cue1-HA
Pgk1
Cue1-HA remaining (%)
WT
opi3Δ
P=0.05
Time of chase (min)
Emc4-HA
Pgk1
Emc4-HA remaining (%)
P=0.002
Nsg2-HA
Pgk1
Nsg2-HA remaining (%)
P=0.01
Sbh1-HA
Pgk1
Sbh1-HA remaining (%)
P=6E-05

Figure 1

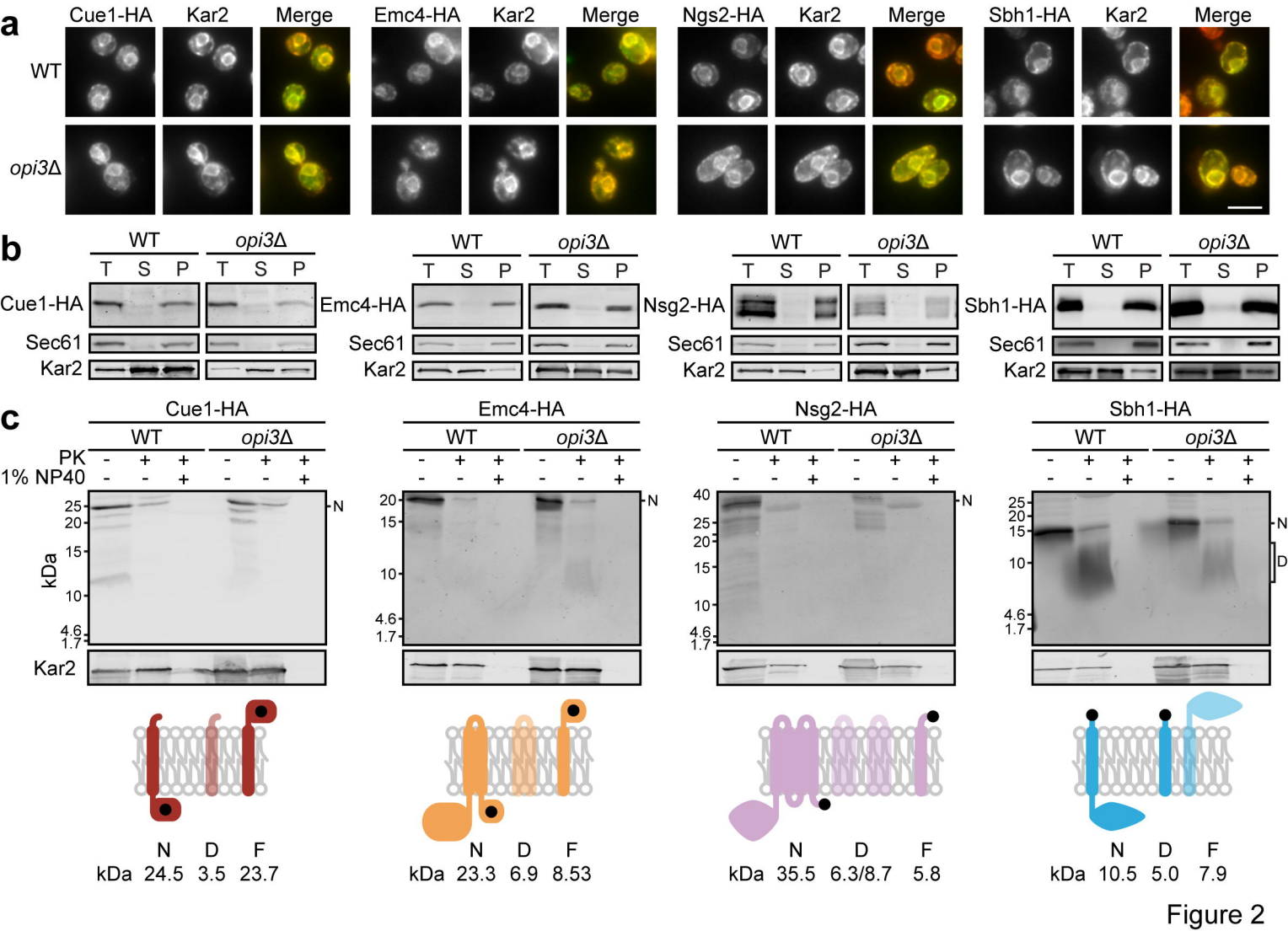
a
Cue1-HA
Kar2
Merge
Emc4-HA
Kar2
Merge
Ngs2-HA
Kar2
Merge
Sbh1-HA
Kar2
Merge
WT
opi3Δ
b
WT
opi3Δ
T S P T S P
Cue1-HA
Sec61
Kar2
Emc4-HA
Nsg2-HA
Sbh1-HA
c
Cue1-HA
Emc4-HA
Nsg2-HA
Sbh1-HA
PK
1% NP40
kDa
N
D
Kar2
N D F
kDa 24.5 3.5 23.7
kDa 23.3 6.9 8.53
kDa 35.5 6.3/8.7 5.8
kDa 10.5 5.0 7.9

Figure 2

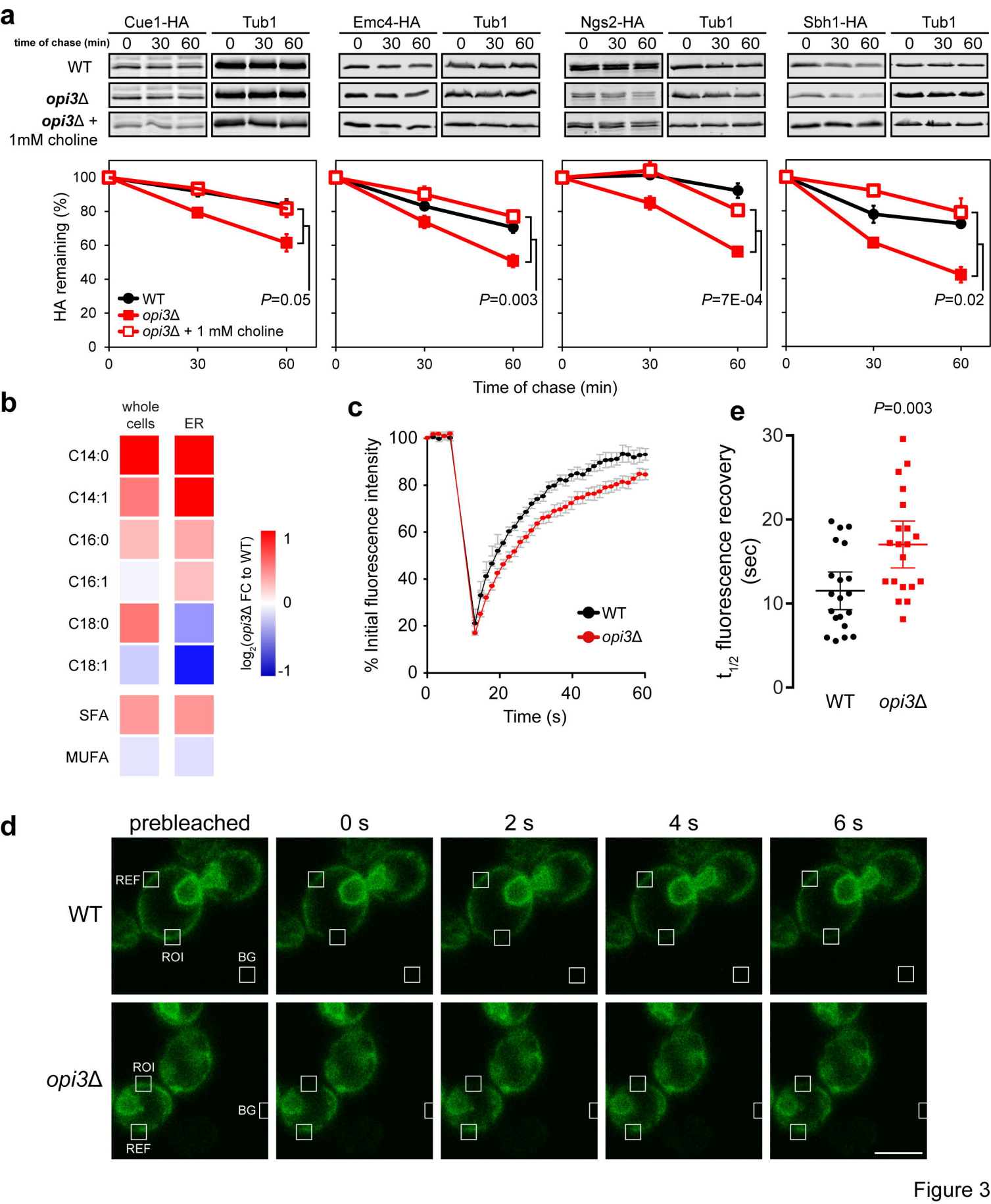
a
Cue1-HA
Tub1
Emc4-HA
Tub1
Ngs2-HA
Tub1
Sbh1-HA
Tub1
time of chase (min)
0 30 60
WT
opi3Δ
opi3Δ + 1mM choline
HA remaining (%)
WT
opi3Δ
opi3Δ + 1 mM choline
P=0.05
P=0.003
P=7E-04
P=0.02
Time of chase (min)
b
whole cells
ER
C14:0
C14:1
C16:0
C16:1
C18:0
C18:1
SFA
MUFA
log2(opi3Δ FC to WT)
c
% Initial fluorescence intensity
WT
opi3Δ
Time (s)
e
P=0.003
t1/2 fluorescence recovery (sec)
WT
opi3Δ
d
prebleached
0 s
2 s
4 s
6 s
WT
opi3Δ
REF
ROI
BG

Figure 3

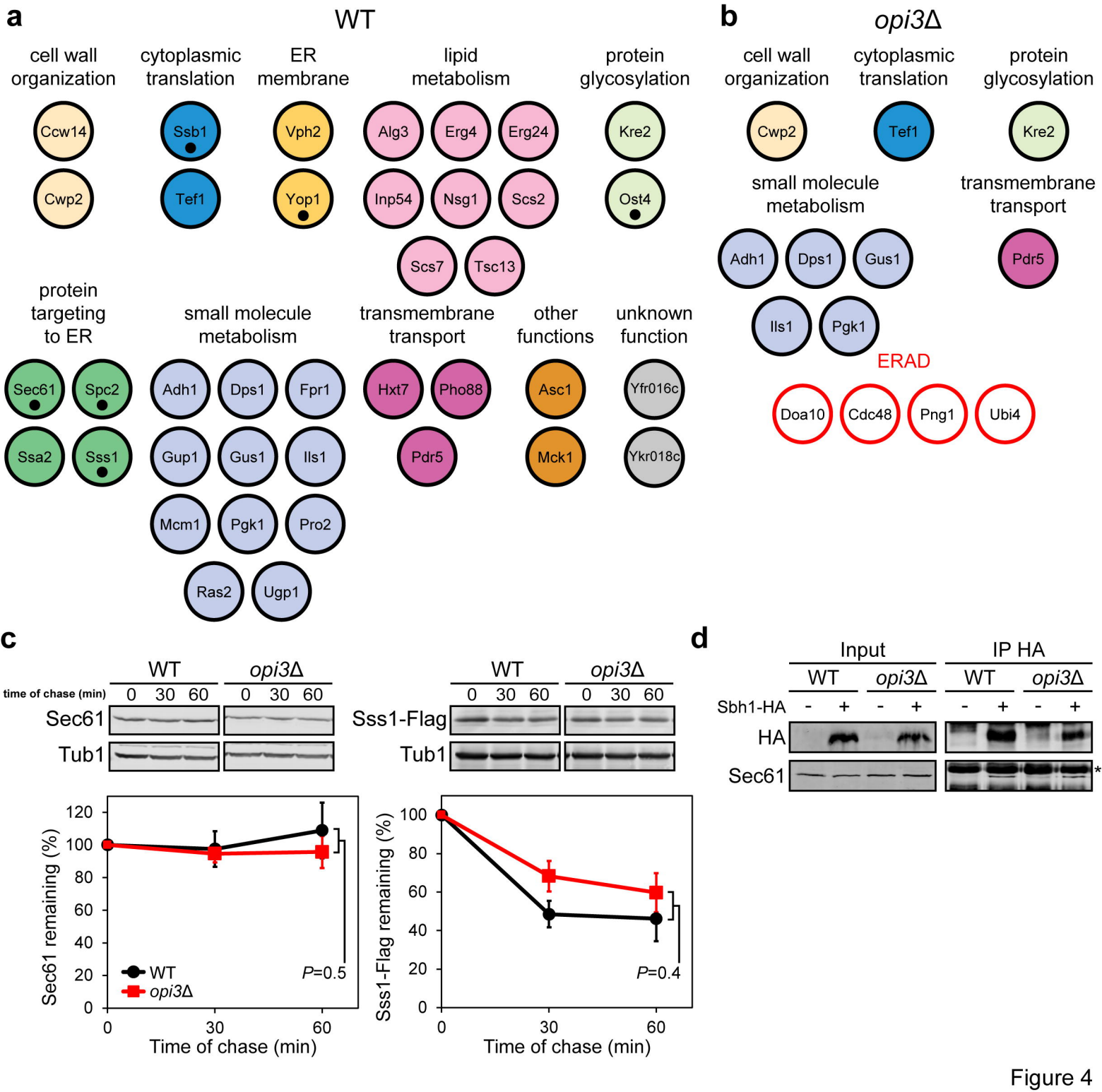
a
WT
cell wall organization
Ccw14
Cwp2
cytoplasmic translation
Ssb1
Tef1
ER membrane
Vph2
Yop1
lipid metabolism
Alg3
Erg4
Erg24
Inp54
Nsg1
Scs2
Scs7
Tsc13
protein glycosylation
Kre2
Ost4
protein targeting to ER
Sec61
Spc2
Ssa2
Sss1
small molecule metabolism
Adh1
Dps1
Fpr1
Gup1
Gus1
Ils1
Mcm1
Pgk1
Pro2
Ras2
Ugp1
transmembrane transport
Hxt7
Pho88
Pdr5
other functions
Asc1
Mck1
unknown function
Yfr016c
Ykr018c
b
opi3Δ
cell wall organization
Cwp2
cytoplasmic translation
Tef1
protein glycosylation
Kre2
small molecule metabolism
Adh1
Dps1
Gus1
Ils1
Pgk1
transmembrane transport
Pdr5
ERAD
Doa10
Cdc48
Png1
Ubi4
c
WT
opi3Δ
time of chase (min)
0 30 60 0 30 60
Sec61
Tub1
Sss1-Flag
Sec61 remaining (%)
Sss1-Flag remaining (%)
WT
opi3Δ
P=0.5
P=0.4
Time of chase (min)
d
Input
IP HA
WT
opi3Δ
Sbh1-HA
HA
Sec61
*

Figure 4

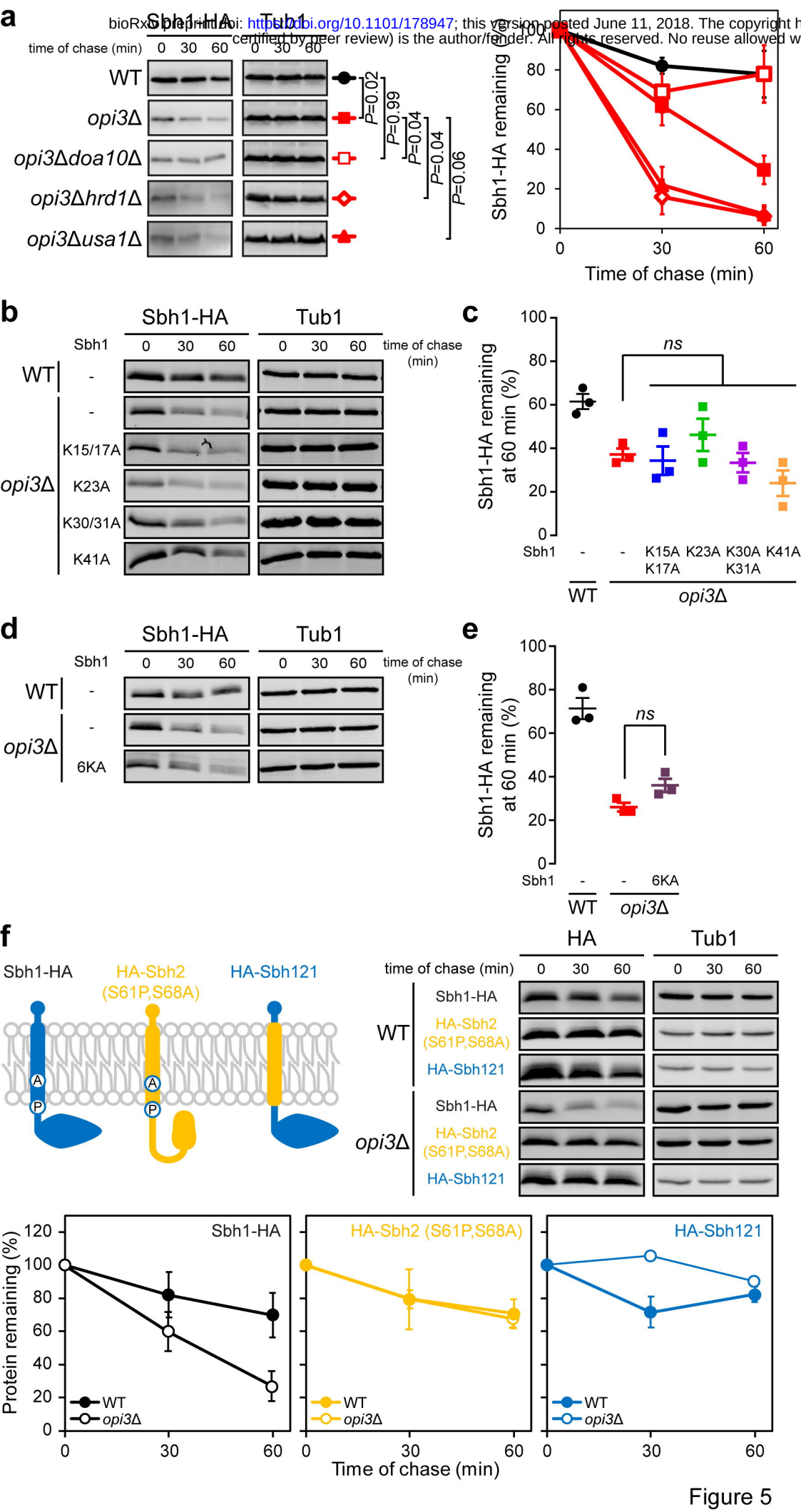

Figure 5

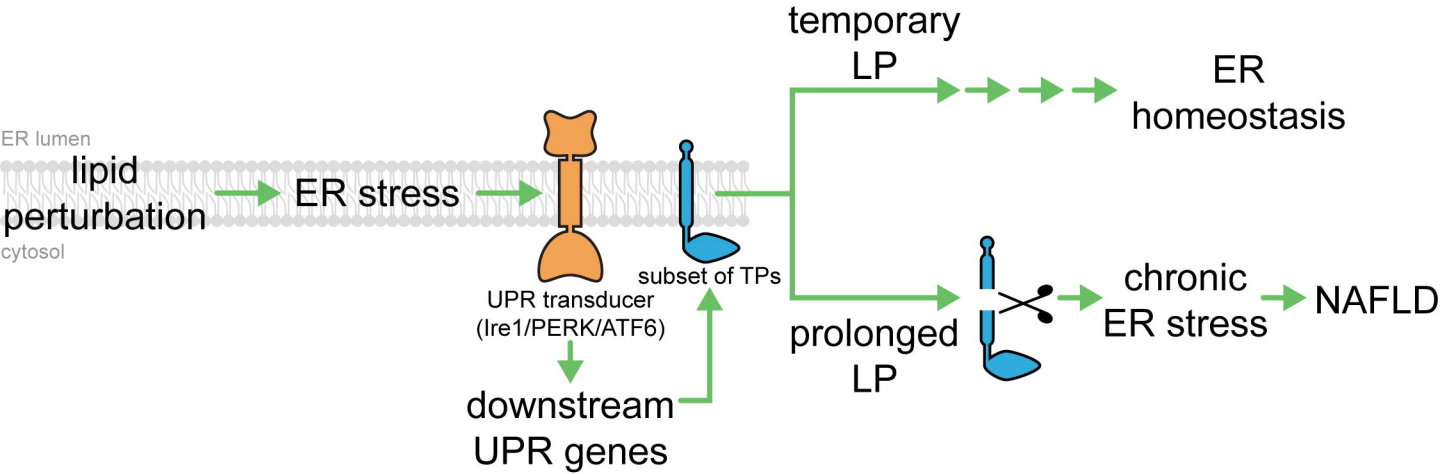
temporary
LP
ER
homeostasis
ER lumen
lipid
perturbation
ER stress
cytosol
subset of TPs
UPR transducer
(Ire1/PERK/ATF6)
chronic
ER stress
NAFLD
prolonged
LP
downstream
UPR genes

Figure 6

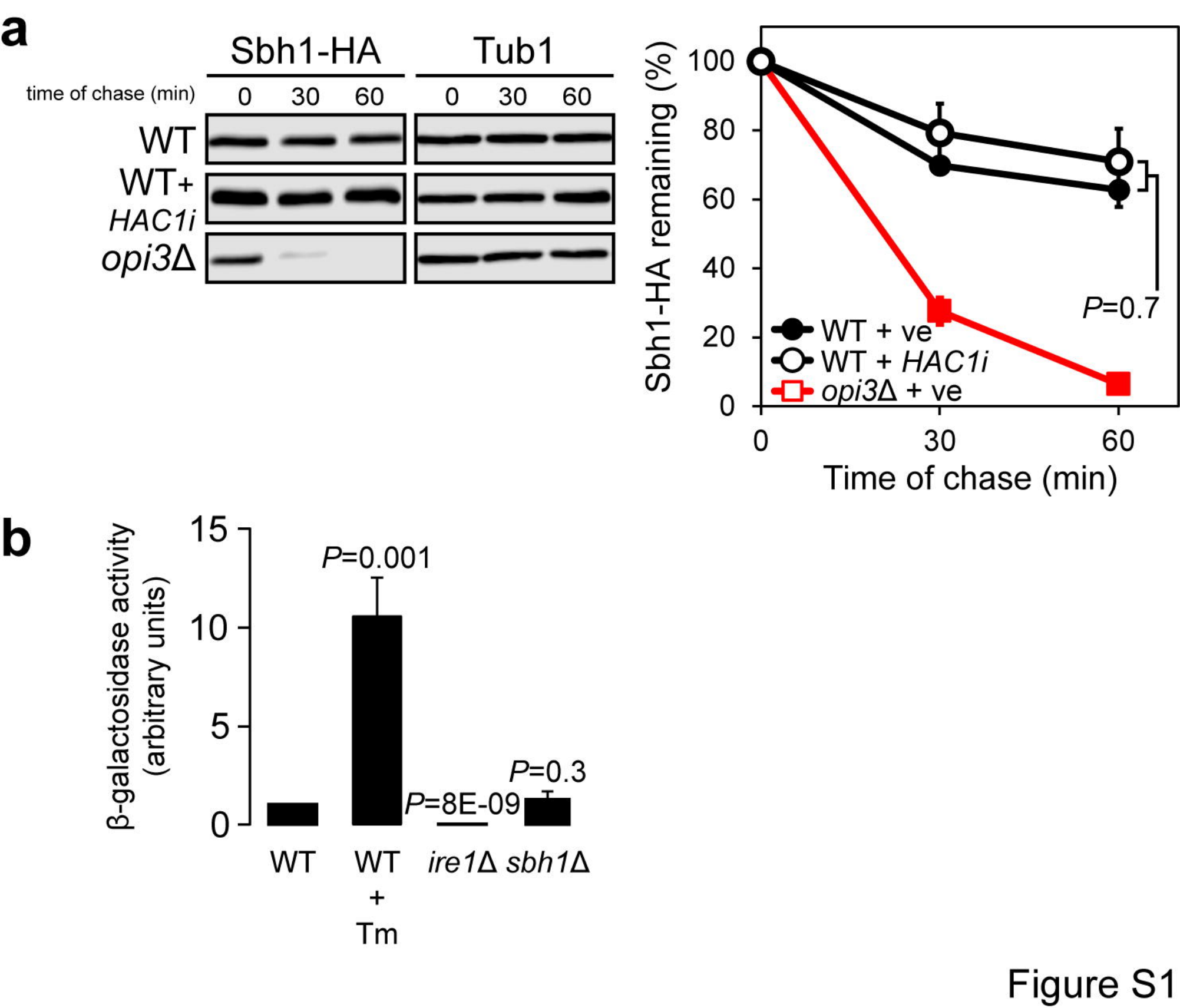
a
Sbh1-HA
Tub1
time of chase (min)
0
30
60
0
30
60
WT
WT+
HAC1i
opi3Δ
Sbh1-HA remaining (%)
100
80
60
40
20
0
P=0.7
WT + ve
WT + HAC1i
opi3Δ + ve
0
30
60
Time of chase (min)
b
β-galactosidase activity
(arbitrary units)
15
10
5
0
P=0.001
P=8E-09
P=0.3
WT
WT
+
Tm
ire1Δ
sbh1Δ

Figure S1

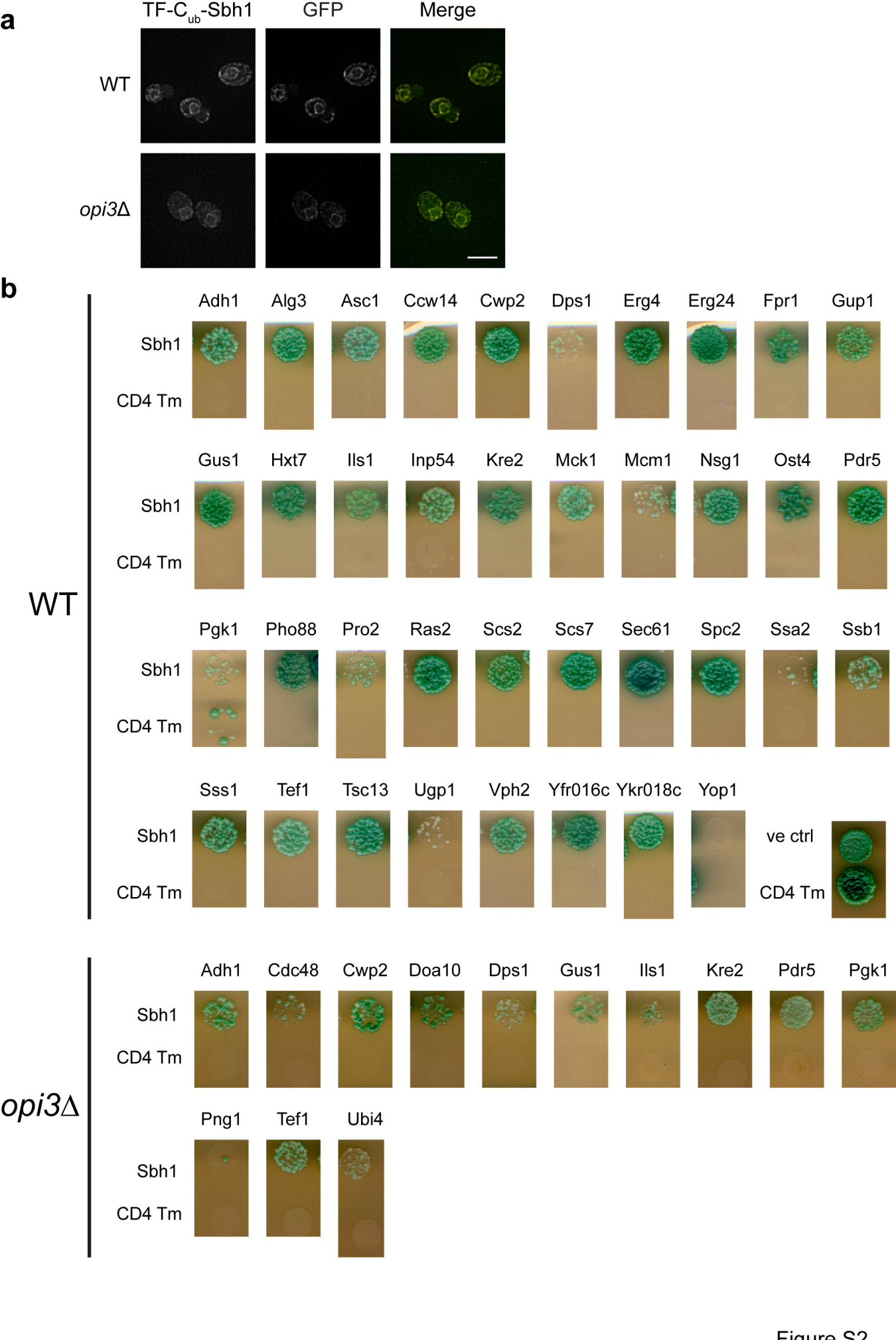
a
TF-Cub-Sbh1
GFP
Merge
WT
opi3Δ
b
WT
Adh1
Alg3
Asc1
Ccw14
Cwp2
Dps1
Erg4
Erg24
Fpr1
Gup1
Sbh1
CD4 Tm
Gus1
Hxt7
Ils1
Inp54
Kre2
Mck1
Mcm1
Nsg1
Ost4
Pdr5
Pgk1
Pho88
Pro2
Ras2
Scs2
Scs7
Sec61
Spc2
Ssa2
Ssb1
Sss1
Tef1
Tsc13
Ugp1
Vph2
Yfr016c
Ykr018c
Yop1
ve ctrl
opi3Δ
Adh1
Cdc48
Cwp2
Doa10
Dps1
Gus1
Ils1
Kre2
Pdr5
Pgk1
Png1
Tef1
Ubi4

Figure S2

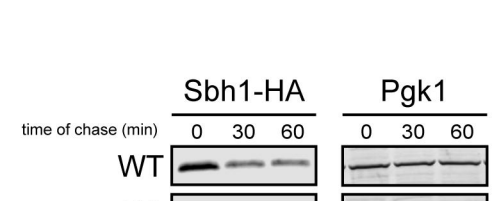
Sbh1-HA
Pgk1
time of chase (min)
0 30 60
0 30 60
WT
opi3Δ
opi3Δcue1Δ
opi3Δpep4Δ

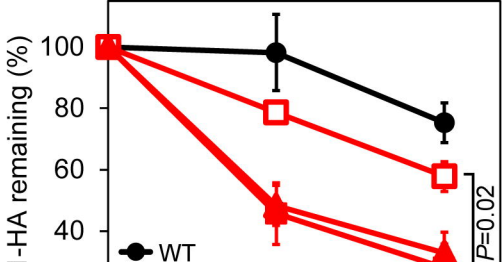
Sbh1-HA remaining (%)
100
80
60
40
20
0
0
30
60
Time of chase (min)
WT
opi3Δ
opi3Δcue1Δ
opi3Δpep4Δ
P=0.02

Figure S3